Diffusion vs. direct transport in the precision of morphogen readout

Sean Fancher[1,2*] **and Andrew Mugler**[1*]

***For correspondence:**
sfancher@sas.upenn.edu (SF);
amugler@purdue.edu (AM)

[1]Department of Physics and Astronomy, Purdue University, West Lafayette, IN 47907, USA; [2]Department of Physics and Astronomy, University of Pennsylvania, Philadelphia, PA 19104, USA

Abstract Morphogen profiles allow cells to determine their position within a developing organism, but not all morphogen profiles form by the same mechanism. Here we derive fundamental limits to the precision of morphogen concentration sensing for two canonical mechanisms: the diffusion of morphogen through extracellular space and the direct transport of morphogen from source cell to target cell, e.g., via cytonemes. We find that direct transport establishes a morphogen profile without adding noise in the process. Despite this advantage, we find that for sufficiently large values of profile length, the diffusion mechanism is many times more precise due to a higher refresh rate of morphogen molecules. We predict a profile lengthscale below which direct transport is more precise, and above which diffusion is more precise. This prediction is supported by data from a wide variety of morphogens in developing organisms.

Introduction

Within developing organisms, morphogen profiles provide cells with information about their position relative to other cells. Cells use this information to determine their position with extremely high precision (***Dubuis et al., 2013***; ***Erdmann et al., 2009***; ***Gregor et al., 2007a***; ***Houchmandzadeh et al., 2002***; ***De Lachapelle and Bergmann, 2010***). However, not all morphogen profiles are formed via the same mechanism, and for some profiles the mechanism is still not well understood. One well-known mechanism is the synthesis-diffusion-clearance (SDC) model in which morphogen molecules are produced by localized source cells and diffuse through extracellular space before degrading or being internalized by target cells (***Akiyama and Gibson, 2015***; ***Gierer and Meinhardt, 1972***; ***Lander et al., 2002***; ***Müller et al., 2013***; ***Rogers and Schier, 2011***; ***Wilcockson et al., 2017***). Alternatively, a direct transport (DT) model has been proposed where morphogen molecules travel through protrusions called cytonemes directly from the source cells to the target cells (***Akiyama and Gibson, 2015***; ***Bressloff and Kim, 2018***; ***Kornberg and Roy, 2014***; ***Müller et al., 2013***; ***Wilcockson et al., 2017***). The presence of these two alternative theories raises the question of whether there exists a difference in the performance capabilities between cells utilizing one or the other.

Experiments have shown that morphogen profiles display many characteristics consistent with the SDC model. The concentration of morphogen as a function of distance from the source cells has been observed to follow an exponential distribution for a variety of different morphogens (***Driever and Nüsslein-Volhard, 1988***; ***Houchmandzadeh et al., 2002***). The accumulation times for several morphogens in *Drosophila* have been measured and found to match the predictions made by the SDC model (***Berezhkovskii et al., 2011***). In zebrafish, the molecular dynamics of the morphogen Fgf8 have been measured and found to be consistent with Brownian diffusion through extracellular space (***Yu et al., 2009***). Despite these consistencies, recent experiments have lent support to the theory that morphogen molecules are transported through cytonemes rather than extracellular

space. The establishment of the Hedgehog morphogen gradient in *Drosophila* is highly correlated in both space and time with the formation of cytonemes (**Bischoff et al., 2013**), while Wnt morphogens have been found to be highly localized around cell protrusions such as cytonemes (**Huang and Kornberg, 2015**; **Stanganello and Scholpp, 2016**). Theoretical studies of both the SDC and DT models have examined these measurable effects (**Berezhkovskii et al., 2011**; **Bressloff and Kim, 2018**; **Shvartsman and Baker, 2012**; **Teimouri and Kolomeisky, 2015**, **2016**), but direct comparisons between the two models have thus far been poorly explored. In particular, it remains unknown whether one model allows for a cell to sense its local morphogen concentration more precisely than the other given biological parameters such as the number of cells or the characteristic lengthscale of the profile.

Here we derive fundamental limits to the precision of morphogen concentration sensing for both the SDC and DT models. We investigate the hypothesis that sensory precision plays a major role in the selection of a gradient formation mechanism during evolution, and we test this hypothesis by quantitatively comparing our theory to morphogen data. Intuitively one might expect the DT model to have less noise due to the fact that molecules are directly deposited at their target. Indeed, we find below that the noise arises only from molecular production and degradation, with no additional noise from molecular transport. However, we also find below that for sufficiently large morphogen profile lengthscales, the SDC model produces less noise than the DT model due to it being able achieve a higher effective unique molecule count. By elucidating the competing effects of profile amplitude, steepness, and noise, we ultimately conclude that there should exist a profile lengthscale below which the DT model is more precise and above which the SDC mechanism is more precise. We find that this prediction is quantitatively supported by data from a wide variety of morphogens, suggesting that readout precision plays an important role in determining the mechanisms of morphogen profile establishment.

Results

Several past studies have focused on the formation dynamics of morphogen profiles (**Berezhkovskii et al., 2011**; **Bressloff and Kim, 2018**; **Shvartsman and Baker, 2012**; **Teimouri and Kolomeisky, 2015**, **2016**). Here we model profiles in the steady state regime, as most of the experimental measurements to which we will later compare our results were taken during stages when the steady state approximation is valid (**Grimm et al., 2010**; **Gregor et al., 2007b**; **Kicheva et al., 2007**; **Yu et al., 2009**; **Kanodia et al., 2009**). Precision depends not only on stochastic fluctuations in the morphogen concentration, but also on the shape of the mean morphogen profile, as the shape determines concentration differences between adjacent cells that may adopt different fates. Therefore, as in past studies (**Gregor et al., 2007a**; **Tostevin et al., 2007**), we define the precision as $P = \Delta\bar{m}_j/\sigma_j$, where σ_j is the standard deviation of the number of morphogen molecules arriving at cell j, and $\Delta\bar{m}_j = \bar{m}_j - \bar{m}_{j+1}$ is the difference between the molecule number in that cell and the adjacent cell. As is typical in studies of both the DT (**Teimouri and Kolomeisky, 2015**; **Bressloff and Kim, 2018**) and SDC (**Berezhkovskii et al., 2011**; **Shvartsman and Baker, 2012**; **Teimouri and Kolomeisky, 2016**) mechanisms, we focus on a one-dimensional line of target cells. However, we derive analogous results for 2D and 3D systems, and we generally find that the dimensionality does not qualitatively change our results, as we discuss later. In 1D, cells extend in both directions from the source cell, with N cells on each side (Fig. 1).[1]

Direct Transport Model

We first consider the DT case, where morphogen molecules are transported via cytonemes that connect a single source cell to multiple target cells (Fig. 1A). Cytonemes are tubular protrusions

[1] We note that in the case of the Bicoid morphogen in the *Drosophila* embryo, target cells extend only on one side of the source. This will introduce a factor of 2 in the means of both the DT and SDC models and a factor slightly greater than 2 in the variance of the SDC model. This will not affect the agreement of the Bicoid data with our theory in Fig. 3C.

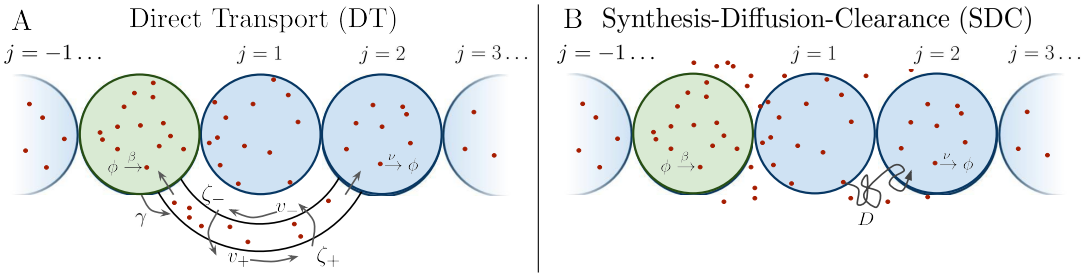

Figure 1. Source cell (green) produces morphogen which is delivered to N target cells (blue) via (A) direct transport (DT) or (B) synthesis-diffusion-clearance (SDC).

that are hundreds of nanometers thick and between several and hundreds of microns long (***Kornberg and Roy, 2014***; ***Kornberg, 2014***). They are supported by actin filaments, and it is thought that morphogen molecules are actively transported along the filaments via molecular motors (***Kornberg and Roy, 2014***; ***Kornberg, 2014***; ***Sanders et al., 2013***; ***Huang and Kornberg, 2015***). It was recently shown that a DT model that includes forward and backward transport of molecules within cytonemes reproduces experimentally measured accumulation times (***Teimouri and Kolomeisky, 2015***; ***Bressloff and Kim, 2018***), although the noise properties of this model were not considered. Here, we review the steady state properties of this model and derive its noise properties.

Consider a single source cell that produces morphogen at rate β. Morphogen molecules enter each cytoneme at rate γ. The cytoneme that leads to the jth target cell has length $2ja$, where a is the cell radius. Once inside a cytoneme, morphogen molecules move forward towards the target cell with velocity v_+ or backwards toward the source cell with velocity v_-, and can switch between these states with rates ζ_+ (forward-to-backward) or ζ_- (backward-to-forward). Once a molecule reaches the forward (backward) end of the cytoneme it is immediately absorbed into the target (source) cell. Molecules within a target cell spontaneously degrade with rate ν. The dynamics of the mean number of morphogen molecules in the source cell $\bar{m}_0(t)$ and jth target cell $\bar{m}_j(t)$, and the mean density of forward-moving molecules $\bar{u}_j^+(x,t)$ and backward-moving molecules $\bar{u}_j^-(x,t)$ in the jth cytoneme are (***Bressloff and Kim, 2018***)

$$\begin{aligned}
\frac{\partial \bar{m}_0}{\partial t} &= \beta - \sum_{j=1}^{N}\left[\gamma \bar{m}_0 - v_- \bar{u}_j^-(0,t)\right],\\
\frac{\partial \bar{u}_j^+}{\partial t} &= -v_+\frac{\partial \bar{u}_j^+}{\partial x} + \zeta_- \bar{u}_j^- - \zeta_+ \bar{u}_j^+ + \gamma \bar{m}_0 \delta(x) - v_+ \bar{u}_j^+ \delta(x - L_j),\\
\frac{\partial \bar{u}_j^-}{\partial t} &= v_-\frac{\partial \bar{u}_j^-}{\partial x} - \zeta_- \bar{u}_j^- + \zeta_+ \bar{u}_j^+ - v_- \bar{u}_j^- \delta(x),\\
\frac{\partial \bar{m}_j}{\partial t} &= v_+ \bar{u}_j^+(L_j,t) - \nu \bar{m}_j.
\end{aligned} \tag{1}$$

The steady-state solution is (***Bressloff and Kim, 2018***)

$$\bar{m}_j^{\rm DT} = \frac{\beta \Gamma_j}{\nu \sum_{k=1}^{N} \Gamma_k}, \text{ where } \Gamma_j = \frac{e^{-2j\kappa a}(1-e^{-\phi})}{1-e^{-\phi-2j\kappa a}}. \tag{2}$$

Here $\gamma\Gamma_j$ is the effective transport rate of morphogen molecules to the jth target cell, and $\phi = \log(d_-/d_+)$ and $\kappa = d_+^{-1} - d_-^{-1}$ are defined in terms of the average distance a molecule would move forward $d_+ = v_+/\zeta_+$ or backward $d_- = v_-/\zeta_-$ within a cytoneme before switching direction. The parameter ϕ sets the shape of Γ_j, and thus of $\bar{m}_j$: when $\phi \ll -1$ the profile is constant, $\Gamma_j = 1$; when $\phi \gg 1$ it is exponential, $\Gamma_j = e^{-2ja/d_+}$; and when $|\phi| \ll 1$ it is a power law for large j, $\Gamma_j = (1+2ja/d_+)^{-1}$.

The parameter κ sets the lengthscale of the profile, defined as

$$\lambda_{\mathrm{DT}} = \sum_{j=1}^{N} \frac{\Gamma_j - \Gamma_N}{\Gamma_1 - \Gamma_N} \approx \frac{1}{|\kappa|} \left(e^{|\phi|} - 1\right) \left(|\phi| - \log\left(e^{|\phi|} - 1\right)\right), \tag{3}$$

where we approximate the sum as an integral for $N \gg 1$. We use this expression to eliminate κ, writing Γ_j in Eq. 2 entirely in terms of ϕ and $\hat{\lambda} \equiv \lambda/a$.

Despite the complexity of the transport process in Eq. 1, we find that it adds no noise to m_j. In fact, here we prove that any system in which molecules can only degrade in the target cells and cannot leave the target cells has the steady-state statistical properties of a simple birth-death process. First consider the special case of only one target cell. Because each morphogen molecule produced in the source cell acts independently of every other morphogen molecule, we define $p(\tau)$ as the probability density that any given molecule will enter the target cell a time τ after it is created in the source cell. Next, we define $Q(\delta t)$ as the probability that a morphogen molecule will enter the target cell between t and $t + \delta t$. This event requires the molecule to have been produced between $t - \tau$ and $t - (\tau + d\tau)$, which occurs with probability $\beta d\tau$; to arrive at the target cell a time τ later and to enter the target cell within the window δt, which occurs with probability $p(\tau)\delta t$; and we must integrate over all possible times τ. Therefore,

$$Q(\delta t) = \int_0^\infty [\beta d\tau][p(\tau)\delta t] = \beta \delta t \int_0^\infty d\tau p(\tau) = \beta \delta t, \tag{4}$$

where the last step follows from normalization. We see that regardless of the form of $p(\tau)$, the probability of a morphogen molecule entering the target cell in any given small time window δt is simply $\beta\delta t$. This result holds regardless of the mechanism by which morphogen molecules go from the source cell to the target cell, as the only effect such a mechanism can have is on $p(\tau)$. This result still holds when the system is expanded to have multiple target cells, as then $p(\tau)$ is replaced with $p_j(\tau)$, the probability density that the molecule enters the jth target cell a time τ after being produced. In this case, $\int_0^\infty d\tau p_j(\tau)$ evaluates to π_j, the total probability the morphogen molecule is ultimately transported to the jth target cell, and $\beta\delta t$ is simply replaced with $\beta\pi_j\delta t$. Combined with the constant degradation rate ν of morphogen molecules within the target cell, this is precisely a birth-death process with birth rate $\beta\pi_j$ and death rate ν. For our system $\pi_j = \Gamma_j / \sum_{k=1}^{N} \Gamma_k$ in Eq. 2.

We now assume that each cell integrates its morphogen molecule count over a time T (***Berg and Purcell, 1977***; ***Gregor et al., 2007a***). The variance in the time average $T^{-1}\int_0^T dt\, m_j(t)$ is simply that of a birth-death process, given by $\sigma_j^2 = 2\bar{m}_j/(T/\tau)$ (***Fancher and Mugler, 2017***), so long as $T \gg \tau$, where $\tau = \nu^{-1}$ is the correlation time. We see that, as expected for a time-averaged Poisson process, the variance increases with the mean $\bar{m}_j$ and decreases with the number T/τ of independent measurements made in the time T. The precision is therefore

$$P_{\mathrm{DT}}^2 = \frac{\bar{m}_j^{\mathrm{DT}} T}{2\tau_{\mathrm{DT}}} \left(\frac{\Delta\bar{m}_j^{\mathrm{DT}}}{\bar{m}_j^{\mathrm{DT}}}\right)^2, \text{ with } \tau_{\mathrm{DT}} = \frac{1}{\nu}. \tag{5}$$

We see that the precision increases with the profile amplitude $\bar{m}_j$, the number of independent measurements T/τ, and the profile steepness $\Delta\bar{m}_j/\bar{m}_j$. The transport process influences the precision only via $\bar{m}_j$, not τ. For a given N, j, and $\hat{\lambda}$, we find that the precision is maximized at a particular $\phi^* > 0$ (Fig. 2A). The reason is that an exponential profile ($\phi \gg 1$) has constant steepness but small amplitude, whereas a power-law profile ($\phi \ll 1$) has low steepness but large amplitude due to its long tail; the optimum is in between.

Synthesis-Diffusion-Clearance Model

We next consider the SDC case (Fig. 1B). Again a single source cell at the origin $x = 0$ produces morphogen at rate β. However, now morphogen molecules diffuse freely along x with coefficient

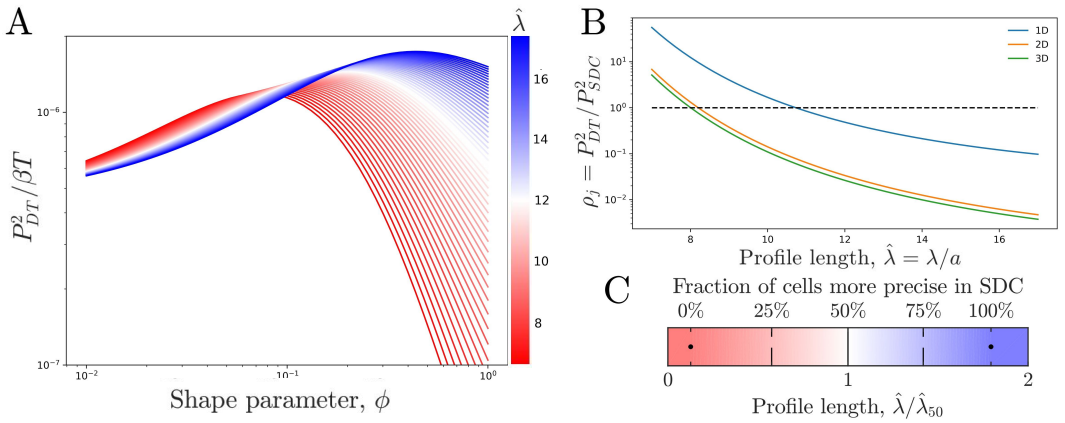

Figure 2. Comparing theoretical DT precision to SDC precision for a single cell. (A) DT precision shows a maximum as a function of shape parameter ϕ for any value of the profile lengthscale. (B) Ratio ρ_j of DT to SDC precision shows a crossover ($\rho_j = 1$) as a function of profile lengthscale λ/a for 1D, 2D, and 3D geometries. Here $j = 50$ is the central cell of $N = 100$ target cells. (C) Percentage of cells for which SDC is more precise ($\rho_j < 1$) in 1D for $N = 100$.

D and degrade spontaneously at any point in space with rate ν. The dynamics of the morphogen concentration $c(x,t)$ are

$$\frac{\partial c}{\partial t} = D\nabla^2 c + \eta_D - \nu c - \eta_\nu + \left(\beta + \eta_\beta\right)\delta(x), \tag{6}$$

where the noise terms associated with diffusion, degradation, and production obey

$$\begin{aligned}\left\langle \eta_D(x',t')\eta_D(x,t)\right\rangle &= 2D\delta(t-t')\vec{\nabla}_x\cdot\vec{\nabla}_{x'}\bar{c}(x)\delta(x-x')\\ \left\langle \eta_\nu(x',t')\eta_\nu(x,t)\right\rangle &= \nu\bar{c}(x)\delta(t-t')\delta(x-x'),\\ \left\langle \eta_\beta(t')\eta_\beta(t)\right\rangle &= \beta\delta(t-t'),\end{aligned} \tag{7}$$

respectively (***Gardiner, 2004***; ***Gillespie, 2000***; ***Fancher and Mugler, 2017***; ***Varennes et al., 2017***). Here $\bar{c}(x) = \beta e^{-x/\lambda}/(\nu\lambda)$ is the steady state mean concentration, with characteristic lengthscale $\lambda_{\text{SDC}} = \sqrt{D/\nu}$. We imagine a target cell located at x that is permeable to the morphogen and counts the number $m(x,t) = \int_V dy\, c(x+y,t)$ of morphogen molecules within its volume V. We use this simpler prescription over explicitly accounting for more realistic mechanisms such as surface receptor binding because it has been shown that the two approaches ultimately yield similar concentration sensing results up to a factor of order unity (***Berg and Purcell, 1977***). For a cell at position $x = 2ja$, the integral evaluates to

$$\bar{m}_j^{\text{SDC}} = 2(\beta/\nu)\sinh(1/\hat{\lambda})e^{-2j/\hat{\lambda}} \tag{8}$$

in steady state.

Because Eq. 6 is linear with Gaussian white noise, calculating the time-averaged variance σ_j^2 is straightforward: we Fourier transform Eq. 6 in space and time, calculate the power spectrum of $m(x,t)$, and take its low-frequency limit (Appendix 1). So long as $T \gg \nu^{-1}$, we obtain the same functional form as Eq. 5,

$$P^2_{\text{SDC}} = \frac{\bar{m}_j^{\text{SDC}} T}{2\tau_{\text{SDC}}}\left(\frac{\Delta\bar{m}_j^{\text{SDC}}}{\bar{m}_j^{\text{SDC}}}\right)^2, \tag{9}$$

because diffusion is a Poisson process. However, here the correlation time is

$$\tau_{\mathrm{SDC}} = \frac{1}{\nu}\left[1 - \frac{(2/\hat{\lambda}) + \sinh(2/\hat{\lambda})}{4\sinh(1/\hat{\lambda})e^{1/\hat{\lambda}}}\right]. \tag{10}$$

The factor in brackets is always less than one and decreases with $\hat{\lambda}$. It reflects the fact that, unlike in the DT model, molecules can leave a target cell not only by degradation, but also by diffusion. Therefore, the rate τ^{-1} at which molecules are refreshed is larger than that from degradation alone. This effect increases the precision because more independent measurements T/τ can be made.

To understand this effect more intuitively, consider a simplified SDC model in which diffusion is modeled as discrete hopping between adjacent target cells at rate h. The autocorrelation function is $C_j(t) = \bar{m}_j I_0(2ht)e^{-(2h+\nu)t}$ (Appendix 2), where I_0 is the zeroth modified Bessel function of the first kind. The correlation time is $\tau = \int_0^\infty dt\, C_j(t)/C_j(0) = [\nu(4h+\nu)]^{-1/2}$, and we see explicitly that it decreases with both degradation (ν) and diffusion (h). In fact, in the limit of fast diffusion ($h \gg \nu$), the expression becomes $\tau = (4\nu h)^{-1/2}$. Correspondingly, in the fast-diffusion limit of Eq. 10 ($\hat{\lambda} \gg 1$), the term in brackets reduces to $\hat{\lambda}^{-1}$, and it becomes $\tau = (\nu\hat{\lambda})^{-1/2} = [4\nu D/(2a)^2]^{-1/2}$. These expressions are identical, with $D/(2a)^2$ playing the role of the hopping rate h, as expected.

Comparing the models

We now ask which model has higher precision. We calculate the precision ratio $\rho_j = P^2_{\mathrm{DT}}/P^2_{\mathrm{SDC}}$ in the jth target cell from Eqs. 2, 5, and 8-10, which depends on j, N, $\hat{\lambda}$, and ϕ. Fig. 2B shows ρ_j as a function of profile length $\hat{\lambda}$ for a cell in the center ($j = N/2$) of a line of $N = 100$ target cells, where for each $\hat{\lambda}$ we use the ϕ^* that maximizes P^2_{DT} as seen in Fig. 2A. We see that for short profiles the DT model is more precise ($\rho_j > 1$) whereas for long profiles the SDC model is more precise ($\rho_j < 1$). This effect holds for a single source cell providing morphogen for a 1D line of target cells as well as for a 1D line of source cells with a 2D sheet of target cells and a 2D sheet of source cells with a 3D volume of target cells.[2]

Fig. 2C shows similar information as Fig. 2B but for all target cells in the line. Specifically, at each $\hat{\lambda}$ value, we find the ϕ^* value that maximizes the percentage of cells for which the DT model is more precise. The color shows the complement: the percentage of cells for which the SDC model is more precise. We normalize the $\hat{\lambda}$ axis by $\hat{\lambda}_{50}$, the value at which this percentage is 50%. As expected, we see that for short profile lengths the DT model is more precise in the majority of cells, whereas for long profiles the SDC model is more precise in the majority of cells.

The reason that the SDC model is more precise for long profiles is that long profiles correspond to fast diffusion, which increases the refresh rate τ^{-1}_{SDC} as discussed above. Conversely, the reason that that the DT model is more precise for short profiles is that it has a larger amplitude. It also has a smaller steepness, but the larger amplitude wins out. Specifically, whereas the SDC amplitude falls off exponentially, $\bar{m}_j \sim e^{-2j/\hat{\lambda}}$, for sufficiently small ϕ^* the DT amplitude falls off as a power law, $\bar{m}_j \sim 1/j$. The steepness $\Delta\bar{m}_j/\bar{m}_j$ of the SDC profile is constant, while the steepness of the DT profile also scales like $1/j$. Thus, the product of the ratio of amplitudes and the square of the ratio of steepnesses, on which ρ_j depends, scales like $e^{2j/\hat{\lambda}}/j^3$. For small $\hat{\lambda}$, the exponential dominates over the cubic for the majority of j values. Consequently, the DT model has the higher precision.

Comparison to Data

We now test our predictions against data for various morphogens. In *Drosophila*, the morphogen Wingless (Wg) is localized near cell protrusions such as cytonemes (***Huang and Kornberg, 2015***; ***Stanganello and Scholpp, 2016***), and the Hedgehog (Hh) gradient correlates highly in both space and time with the formation of cytonemes (***Bischoff et al., 2013***), suggesting that these two morphogen profiles are formed via a DT mechanism. Conversely, Bicoid has been understood as a model example of SDC for decades (***Driever and Nüsslein-Volhard, 1988***; ***Gregor et al., 2007a***;

[2] For the DT model, the 2D and 3D cases are identical to the 1D case as we assume that cytonemes extend perpendicular to the source cells; for the SDC model see Appendix 1.

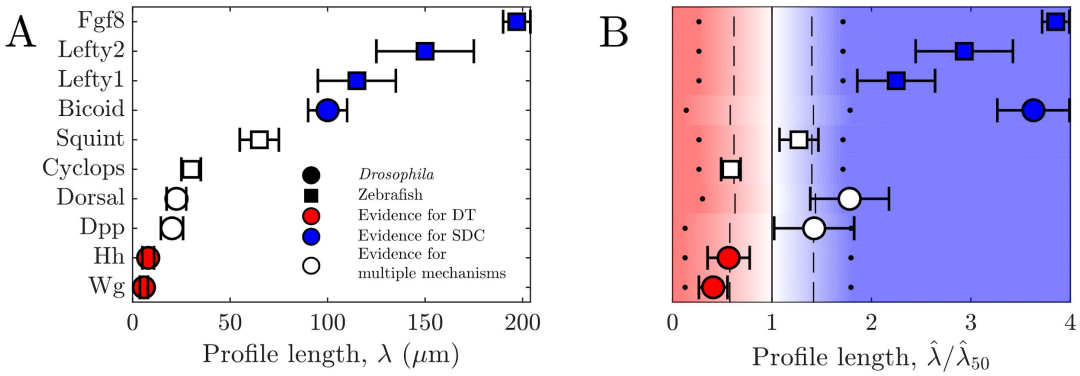

Figure 3. Comparing theory and experiment. (A) λ values for morphogens estimated from experiments, colored by whether experiments support a DT (red), SDC (blue), or multiple mechanisms (white). (B) Data from A overlaid with color from theory using values of a and N estimated from experiments. Color is as in Fig. 2C indicating percentage of cells for which SDC is predicted to be more precise.

Houchmandzadeh et al., 2002). Similarly, Dorsal is spread by diffusion, however its absorption is localized to a specific region of target cells via a nonuniform degradation mechanism, making it more complex than the simple SDC model (***Carrell et al., 2017***). Finally, for Dpp there is evidence for a variety of different gradient formation mechanisms (***Akiyama and Gibson, 2015***; ***Müller et al., 2013***; ***Wilcockson et al., 2017***).

In zebrafish, the morphogen Fgf8 has been studied at the single molecule level and found to have molecular dynamics closely matching the Brownian movement expected in an SDC mechanism (***Yu et al., 2009***). Similarly, Cyclops, Squint, Lefty1, and Lefty2, all of which are involved in the Nodal/Lefty system, have been shown to spread diffusively and affect cells distant from their source (***Müller et al., 2013***; ***Rogers and Müller, 2018***). This would support the SDC mechanism, although Cyclops and Squint have been argued to be tightly regulated via a Gierer-Meinhardt type system, thus diminishing their gradient sizes to values much lower than what they would be without this regulation (***Gierer and Meinhardt, 1972***; ***Rogers and Müller, 2018***).

For all of these morphogens, we estimate the profile lengthscales λ from the experimental data (***Kicheva et al., 2007***; ***Wartlick et al., 2011***; ***Gregor et al., 2007b***,a; ***Liberman et al., 2009***; ***Yu et al., 2009***; ***Müller et al., 2012***) (Appendix 3). Fig. 3A shows these λ values and indicates for each morphogen whether the evidence described above suggests a DT mechanism (red), an SDC mechanism (blue), or multiple mechanisms including DT and SDC (white). We see that in general, the three cases correspond to short, long, and intermediate profile lengths, respectively, which is qualitatively consistent with our predictions.

To make the comparison quantitative, we estimate the values of cell radius a and cell number N from the experimental data (***Kicheva et al., 2007***; ***Gregor et al., 2007a***; ***Liberman et al., 2009***; ***Yu et al., 2009***; ***Kimmel et al., 1995***) (Appendix 3) in order to calculate ρ_j from our theory in each case. The background color in Fig. 3B shows the percentage of cells for which we predict that the SDC model is more precise as a function of $\hat{\lambda}$ as in Fig. 2C. The data points in Fig. 3B show the values of $\hat{\lambda}$ from the experiments, also normalized by $\hat{\lambda}_{50}$ from the theory. For each morphogen species we assume a 1D system for simplicity as we have checked that considering higher dimensions yields negligible differences to the results presented in Fig. 3B. We see that our theory predicts the correct threshold: the morphogens for which the evidence suggests either a DT or an SDC mechanism (red or blue) fall into the regime in which we predict that mechanism to be more precise for most of the cells, and the morphogens with multiple mechanisms (white) fall in between. This result provides quantitative support for the idea that morphogen profiles form according to the mechanism that maximizes the sensory precision of the target cells.

Discussion

We have shown that in the steady-state regime, the DT and SDC models of morphogen profile formation yield different scalings of readout precision with the length of the profile and population size. As a result, there exist regimes in this parameter space in which either mechanism is more precise. While the DT model benefits from larger molecule numbers and no added noise from the transport process, the ability of molecules to diffuse into and away from a target cell in the SDC model allows the cell to measure a greater number of effectively unique molecules in the same time frame. By examining how these phenomena affect the cells' sensory precision, we predicted that morphogen profiles with shorter lengths should utilize cytonemes or some other form of direct transport mechanism, whereas morphogens with longer profiles should rely on extracellular diffusion, a prediction that is in quantitative agreement with measurements on known morphogens. It will be interesting to observe whether this trend is further strengthened as more experimental evidence is obtained for different morphogens, as well as to expand the theory of multicellular concentration sensing to further biological contexts.

Despite the quantitative agreement between our theory and experiments, it is clear that the models presented here are minimal and thus cannot be directly applied to all systems. This is exemplified by morphogen such as Dorsal, which due to aforementioned diffusive spreading and nonuniform degradation mechanism clearly does not strictly follow either model. Additionally, the SDC model can be violated if the diffusion of morphogen through a biological environment is hindered by the typically crowded nature of such environments, leading to possibly subdiffusive behavior (***Ellery et al., 2014***; ***Fanelli and McKane, 2010***). For the DT model, we explicitly ignored the dynamics of the cytonemes themselves due to the growth rate of the cytonemes being sufficiently fast so as to traverse the entire system size in significantly less time than is required for the cells to integrate their morphogen counts over (***Bischoff et al., 2013***; ***Chen et al., 2017***). This assumption is problematic if cytonemes continue to behave dynamically after reaching the source cell. In particular, the process of cytonemes switching between phases of growing and retracting can introduce super-Poissonian noise sources to the morphogen count within the target cells. It will be interesting to explore the implications of each of these complications in future works.

Acknowledgments

We thank Chris Bairnsfather for useful discussions.

Appendix 1: Time-averaged variance in the SDC model

Here we calculate the time-averaged variance of the morphogen molecule number using the low-frequency limit of the power spectrum. We first introduce the power spectrum, and then we calculate the variance for the 1D, 2D, and 3D geometries.

Power Spectrum

We first discuss the correlation function and power spectrum to establish some definitions and notation. Specifically, we show that the variance in the long-time average of a variable is given by the low-frequency limit of its power spectrum. For a one dimensional function $x(t)$ with mean 0, the correlation function $C(t)$ takes the form

$$C\left(t-t'\right)=\left\langle x\left(t'\right)x\left(t\right)\right\rangle . \tag{11}$$

Since absolute time is irrelevant in the steady state of any physical system with no time dependent forcing, t' can be set to 0 without loss of generality. This leads to a definition for the power spectrum of $x(t)$ as

$$S(\omega) = \int \frac{d\omega'}{2\pi} \left\langle \tilde{x}^*(\omega') \tilde{x}(\omega) \right\rangle = \frac{1}{2\pi} \int d\omega' dt dt' \left\langle x(t') x(t) \right\rangle e^{i\omega t} e^{-i\omega' t'}$$
$$= \int dt dt' C(t-t') e^{i\omega t} \delta(t') = \int dt C(t) e^{i\omega t}. \quad (12)$$

Thus, under this definition the power spectrum is seen to be the Fourier transform of the correlation function. Additionally, when $x(t)$ is averaged over a time T, the time averaged correlation function of $x(t)$ takes the form

$$C_T(t-t') = \left\langle \left(\frac{1}{T} \int_{t'}^{t'+T} d\tau' x(\tau') \right) \left(\frac{1}{T} \int_{t}^{t+T} d\tau x(\tau) \right) \right\rangle$$
$$= \frac{1}{T^2} \int_{t}^{t+T} d\tau \int_{t'}^{t'+T} d\tau' \left\langle x(\tau') x(\tau) \right\rangle$$
$$= \frac{1}{T^2} \int_{t}^{t+T} d\tau \int_{t'}^{t'+T} d\tau' C(\tau - \tau'). \quad (13)$$

Let $y \equiv (\tau - \tau') - (t - t')$ and $z \equiv (\tau + \tau') - (t + t')$. This transforms Eq. 13 into

$$C_T(t-t') = \frac{1}{T^2} \int_{-T}^{T} dy \int_{|y|}^{2T-|y|} dz \frac{1}{2} C(y + t - t')$$
$$= \frac{1}{T^2} \int_{-T}^{T} dy (T - |y|) C(y + t - t'). \quad (14)$$

By inverting the relationship found in Eq. 12, $C(y + t - t')$ can be replaced with an inverse Fourier transform of $S(\omega)$ to produce

$$C_T(t-t') = \frac{1}{T^2} \int_{-T}^{T} dy \int \frac{d\omega}{2\pi} (T - |y|) S(\omega) e^{-i\omega(y+t-t')}$$
$$= \int \frac{d\omega}{2\pi} \left(\frac{2}{\omega T} \sin\left(\frac{\omega T}{2} \right) \right)^2 S(\omega) e^{-i\omega(t-t')}. \quad (15)$$

The factor of $(\omega T)^{-2}$ in the integrand of Eq. 15 forces only small values of ω to contribute when T is large. Thus, the approximation $S(\omega) \approx S(0)$ can be made since only values of ω near 0 are contributing. This causes $C_T(0)$, which we will denote as σ^2 through this and the main text, to be exactly calculable to

$$\sigma^2 = C_T(0) \approx S(0) \int \frac{d\omega}{2\pi} \left(\frac{2}{\omega T} \sin\left(\frac{\omega T}{2} \right) \right)^2 = \frac{S(0)}{T}. \quad (16)$$

Of important note is the fact that this approximation only works if $S(\omega)$ varies slowly compared to $(2\sin(\omega T/2)/\omega T)^2$ near $\omega = 0$. Since $C(t)$ must be time symmetric, $S(\omega)$ must also be symmetric and thus an even function of ω. Thus, near $\omega = 0$ the lowest order correction term for each function will be the second order term. Normalizing each term by the 0-frequency value of each function then lets us to impose the condition

$$\left| \frac{1}{S(0)} \frac{\partial^2 S(\omega)}{\partial \omega^2} \bigg|_{\omega=0} \right| \ll \left| \frac{\partial^2}{\partial \omega^2} \left(\frac{2}{\omega T} \sin\left(\frac{\omega T}{2} \right) \right)^2 \bigg|_{\omega=0} \right| = \frac{T^2}{6}. \quad (17)$$

So long as this condition is satisfied, the approximation given in Eq. 16 is valid.

We now cast Eq. 16 into a more intuitive form by considering the correlation time τ, which can be defined as

$$\tau = \int_0^\infty dt \frac{C(t)}{C(0)}. \tag{18}$$

Continuing the use the fact that $C(t)$ must be time symmetric and thus an even function of t, Eq. 12 can be used to produce the result

$$S(0) = \int dt C(t) = 2\int_0^\infty dt C(t) = 2\tau C(0). \tag{19}$$

Inserting this result into Eq. 16 produces

$$\sigma^2 \approx \frac{2\tau}{T} C(0), \tag{20}$$

thus relating the long-time averaged variance, σ^2, to the instantaneous variance, $C(0)$, and the number of correlation times the system averages over, T/τ.

Variance and precision

We now consider a model for the Synthesis-Diffusion-Clearance system. We still assume there is a single source cell which produces morphogen at rate β, but now the morphogen is released into the extracellular environment where it freely diffuses at rate D. The morphogen can also spontaneously degrade at rate ν. Even though in the main text we focus on a zero-dimensional source in a one-dimensional space, here we will look at diffusion in a multitude of different spaces with different dimensions as well as morphogen sources that span a multitude of different dimensions. In each case, the sources will secrete morphogen molecules into a density field c which must follow

$$\frac{\partial c}{\partial t} = D\nabla^2 c + \eta_D - \nu c - \eta_\nu + \left(\beta + \eta_\beta\right)\delta^{SP-SO}\left(\vec{x}\right), \tag{21}$$

where SP is the number of spatial dimensions, SO is the dimensionality of the source, and ∇^2 is taken over all SP dimensions. Each η term is a Langevin noise term that represents Gaussian white noise for the diffusion, degradation, and production processes respectively. Of important note is that $\delta^{SP-SO}\left(\vec{x}\right)$ is a δ function only in the **last** $SP-SO$ dimensions of the space. So, for example, if there was a 1 dimensional source in 3 dimensional space, then $\delta^{3-1}\left(\vec{x}\right)$ would be a δ function in the $\hat{y}$ and $\hat{z}$ directions but not the $\hat{x}$ direction. This means that β and η_β will have units of $T^{-1}L^{-SO}$, where T is time and L is space.

We can now assume c has reached a steady state and separate it into $c = \bar{c} + \delta c$, which in turn allows Eq. 21 to separate into

$$0 = D\nabla^2\bar{c} - \nu\bar{c} + \beta\delta^{SP-SO}\left(\vec{x}\right) \tag{22}$$

$$\frac{\partial \delta c}{\partial t} = D\nabla^2\delta c + \eta_D - \nu\delta c - \eta_\nu + \eta_\beta\delta^{SP-SO}\left(\vec{x}\right). \tag{23}$$

Fourier transforming Eq. 22 in space and dividing it by ν then yields

$$0 = -\lambda^2\left|\vec{k}\right|^2\tilde{\bar{c}} - \tilde{\bar{c}} + \frac{\beta}{\nu}\left(2\pi\right)^{SO}\delta^{SO}\left(\vec{k}\right) \implies \tilde{\bar{c}} = \frac{\beta}{\nu}\frac{\left(2\pi\right)^{SO}\delta^{SO}\left(\vec{k}\right)}{1+\lambda^2\left|\vec{k}\right|^2}, \tag{24}$$

where

$$\lambda = \sqrt{\frac{D}{\nu}}. \tag{25}$$

Of similarly important note is that $\delta^{SO}\left(\vec{k}\right)$ is a δ function only in the **first** SO dimensions of k-space. So in the 1 dimensional source, 3 dimensional space example $\delta^{SO}\left(\vec{k}\right)$ would be a δ function in the $\hat{x}$ direction of k-space but not the $\hat{y}$ or $\hat{z}$ directions.

This allows $\bar{c}$ to be written as

$$\begin{aligned}\bar{c}\left(\vec{x}\right) &= \int \frac{d^{SP}k}{\left(2\pi\right)^{SP}} e^{-i\vec{k}\cdot\vec{x}} \tilde{\bar{c}}\left(\vec{k}\right) = \frac{\beta}{\nu}\int \frac{d^{SP}k}{\left(2\pi\right)^{SP}} e^{-i\vec{k}\cdot\vec{x}} \frac{\left(2\pi\right)^{SO}\delta^{SO}\left(\vec{k}\right)}{1+\lambda^2\left|\vec{k}\right|^2} \\ &= \frac{\beta}{\nu}\int \frac{d^{SP-SO}k}{\left(2\pi\right)^{SP-SO}} e^{-i\vec{k}\cdot\vec{x}} \frac{1}{1+\lambda^2\left|\vec{k}\right|^2} = \frac{\beta\lambda^{-(SP-SO)}}{\nu} P_{SP-SO}\left(\frac{\left|\vec{x}\right|}{\lambda}\right),\end{aligned} \tag{26}$$

where

$$P_N\left(x\right) = \int \frac{d^N u}{\left(2\pi\right)^N} e^{-i\vec{u}\cdot\vec{x}} \frac{1}{1+\left|\vec{u}\right|^2}. \tag{27}$$

It is important to note that P_N does not integrate over all available dimensions, but only over the last N dimensions of the space. This in turn means that its argument can only depend on the last N dimensions of any input vector. Returning to the 1 dimensional source, 3 dimensional space example, $P_{3-1}\left(\left|\vec{x}\right|/\lambda\right)$ should only take the y and z components of $\vec{x}$ into account. The x component is made irrelevant by the translational symmetry of the system along the x-axis.

Moving on to the noise terms, Eq. 23 can be Fourier transformed in space and time to yield

$$-i\omega\tilde{\delta c} = -D\left|\vec{k}\right|^2\tilde{\delta c} + \tilde{\eta}_D - \nu\tilde{\delta c} - \tilde{\eta}_\nu + \tilde{\eta}_\beta \implies \tilde{\delta c} = \frac{\tilde{\eta}_D - \tilde{\eta}_\nu + \tilde{\eta}_\beta}{\nu\left(1+\lambda^2\left|\vec{k}\right|^2 - i\frac{\omega}{\nu}\right)}, \tag{28}$$

where $\eta_\beta\left(\vec{k},\omega\right)$ depends only on the first SO dimensions of k-space. Assuming the η terms are all independent of each other allows the cross spectrum of c to be

$$\begin{aligned}\left\langle \tilde{\delta c}^*\left(\vec{k}',\omega'\right)\tilde{\delta c}\left(\vec{k},\omega\right)\right\rangle &= \frac{1}{\nu^2\left(1+\lambda^2\left|\vec{k}\right|^2 - i\frac{\omega}{\nu}\right)\left(1+\lambda^2\left|\vec{k}'\right|^2 + i\frac{\omega'}{\nu}\right)} \\ &\cdot\left(\left\langle\tilde{\eta}_D^*\left(\vec{k}',\omega'\right)\tilde{\eta}_D\left(\vec{k},\omega\right)\right\rangle + \left\langle\tilde{\eta}_\nu^*\left(\vec{k}',\omega'\right)\tilde{\eta}_\nu\left(\vec{k},\omega\right)\right\rangle + \left\langle\tilde{\eta}_\beta^*\left(\vec{k}',\omega'\right)\tilde{\eta}_\beta\left(\vec{k},\omega\right)\right\rangle\right).\end{aligned} \tag{29}$$

The cross spectrum of η_D can be obtained from its correlation function. To derive such a correlation function, we first consider a separate Markovian system comprised of a 1-dimensional lattice of discrete compartments that a diffusing species Y can exist in. The dimensionality is chosen purely for simplicity, as the method outlined below can be easily generalized to higher dimensions to produce the same result. Let $y_i\left(t\right)$ be the number of Y molecules in the ith compartment at time t and d be the rate at which these molecules move to the $i-1$ or $i+1$ compartment. Given a sufficiently small time step δt, the probability of a molecule moving from the ith compartment to the $i\pm1$ compartment is

$$P\left(\left\{y_i\left(t+\delta t\right), y_{i\pm1}\left(t+\delta t\right)\right\} = \left\{y_i\left(t\right)-1, y_{i\pm1}\left(t\right)+1\right\}\right) = y_i\left(t\right)d\delta t. \tag{30}$$

Higher order interactions in which multiple molecules are transfered within the time step δt will have probabilites of order $\left(\delta t\right)^2$ or higher and can thus be ignored. This allows the mean of $\delta y_i\left(t\right) = y_i\left(t+\delta t\right) - y_i\left(t\right)$ to take the form

$$\left\langle\delta y_i\left(t\right)\right\rangle = \left(y_{i-1}\left(t\right) + y_{i+1}\left(t\right) - 2y_i\left(t\right)\right)d\delta t, \tag{31}$$

where the first two terms come from molecules moving into the ith compartment from the $i-1$ and $i+1$ compartments respectively and the third term comes from the two different ways molecules can leave the ith compartment. As δt is small, each of these transfer processes can be treated as being Poissonianly distributed. This allows the variance of $\delta y_i(t)$ to simply be the right-hand side of Eq. 31 but with each term taken to be its absolute value so there are no subtractions. Additionally, this approximation allows the covariance between δy_i and $\delta y_{i\pm1}$ to be taken as the negative of the sum of the expected number of molecules moving from the ith compartment to the $i\pm1$ compartment and vice versa. With these, the correlation function between $\delta y_i(t)$ and $\delta y_j(t)$ can be written as

$$\left\langle \delta y_j(t)\,\delta y_i(t)\right\rangle = \left(y_{i-1}(t)+y_{i+1}(t)+2y_i(t)\right)d\delta t\delta_{i,j} - \left(y_i(t)+y_{i-1}(t)\right)d\delta t\delta_{i-1,j} - \left(y_i(t)+y_{i+1}(t)\right)d\delta t\delta_{i+1,j}. \tag{32}$$

We now take the system to continuous space by letting $y_i(t)\to\ell c(x,t)$ and $\delta_{i,j}\to\ell\delta\left(x-x'\right)$ with any intances of ±1 in the indices also being converted to $\pm\ell$. Putting these substitutions into Eq. 32 and dividing by $\left(\ell\delta t\right)^2$ yields

$$\begin{aligned}\left\langle \frac{\delta c\left(x',t\right)}{\delta t}\frac{\delta c(x,t)}{\delta t}\right\rangle &= \frac{d}{\delta t}\left(\left(c\left(x-\ell,t\right)+c\left(x+\ell,t\right)+2c(x,t)\right)\delta\left(x-x'\right)-\left(c(x,t)+c\left(x-\ell,t\right)\right)\delta\left(x-\ell-x'\right)\right.\\ &\qquad\left.-\left(c(x,t)+c\left(x+\ell,t\right)\right)\delta\left(x+\ell-x'\right)\right)\\ &= \frac{d}{\delta t}\left(\left(c\left(x+\ell,t\right)\delta\left(x-x'\right)-c\left(x+\ell,t\right)\delta\left(x+\ell-x'\right)\right)-\left(c(x,t)\delta\left(x-\ell-x'\right)-c(x,t)\delta\left(x-x'\right)\right)\right.\\ &\qquad\left.\left(c(x,t)\delta\left(x-x'\right)-c(x,t)\delta\left(x+\ell-x'\right)\right)-\left(c\left(x-\ell,t\right)\delta\left(x-\ell-x'\right)-c\left(x-\ell,t\right)\delta\left(x-x'\right)\right)\right).\end{aligned} \tag{33}$$

Eq. 33 has been rearranged into this form so as to easily apply the operators $\partial_x^{\pm}$ defined as

$$\partial_x^+ f(x) = \frac{f\left(x+\ell\right)-f(x)}{\ell}, \tag{34a}$$

$$\partial_x^- f(x) = \frac{f(x)-f\left(x-\ell\right)}{\ell}. \tag{34b}$$

Using this notation, Eq. 33 can be simplfied into

$$\begin{aligned}\left\langle \frac{\delta c\left(x',t\right)}{\delta t}\frac{\delta c(x,t)}{\delta t}\right\rangle &= \frac{\ell d}{\delta t}\left(\partial_x^+\left(c(x,t)\delta\left(x-\ell-x'\right)-c(x,t)\delta\left(x-x'\right)\right)\right.\\ &\qquad\left.+\partial_x^-\left(c(x,t)\delta\left(x-x'\right)-c(x,t)\delta\left(x+\ell-x'\right)\right)\right)\\ &= \frac{\ell^2 d}{\delta t}\left(\partial_x^+\partial_{x'}^+ + \partial_x^-\partial_{x'}^-\right)\left(c(x,t)\delta\left(x-x'\right)\right).\end{aligned} \tag{35}$$

Taking the $\ell\to0$ limit while holding $D=\ell^2 d$ constant allows $\partial_x^{\pm}$ and $\partial_{x'}^{\pm}$ to converge to true derivatives, ∂_x and $\partial_{x'}$. Additionally, if the $\delta c\left(x',t\right)/\delta t$ term on the left-hand side of Eq. 35 is replaced with $\delta c\left(x',t'\right)/\delta t$ for $t'\neq t$, then the entire right-hand side must go to 0 as the system is Markovian. This can be accomplished by multiplying the right-hand side by a factor of $\delta_{t,t'}$. Taking the $\delta t\to0$ limit then turns the two terms on the left-hand side into true derivatives in time, ∂_t and $\partial_{t'}$, acting on $c(x,t)$ and $c\left(x',t'\right)$ respectively while the factor of $\delta_{t,t'}/\delta t$ on the right-hand side becomes $\delta\left(t-t'\right)$. Altogether, this transforms Eq. 35 into

$$\left\langle \partial_{t'}c\left(x',t'\right)\partial_t c(x,t)\right\rangle = 2D\delta\left(t-t'\right)\partial_x\partial_{x'}\left(c(x,t)\delta\left(x-x'\right)\right). \tag{36}$$

Finally, by approximating the system as being in steady state, $c(x,t)$ can be replaced with $\bar{c}(x)$ and $\partial_t c(x,t)$ becomes equivalent to $\eta_D(x,t)$. Making these substitutions and generalizing Eq. 36 to arbitrary dimensions yields

$$\left\langle \eta_D\left(\vec{x}',t'\right)\eta_D\left(\vec{x},t\right)\right\rangle = 2D\delta\left(t-t'\right)\vec{\nabla}\cdot\vec{\nabla}'\left(\bar{c}\left(\vec{x}\right)\delta^{SP}\left(\vec{x}-\vec{x}'\right)\right). \tag{37}$$

Fourier transforming Eq. 37 can be easily performed due to the δ functions, integrating the spatial terms by parts, and utilizing Eq. 24 to yield

$$\begin{aligned}
\left\langle \tilde{\eta}_D^*\left(\vec{k}',\omega'\right)\tilde{\eta}_D\left(\vec{k},\omega\right)\right\rangle &= \int d^{SP}xd^{SP}x'dtdt'e^{i\vec{k}\cdot\vec{x}}e^{-i\vec{k}'\cdot\vec{x}'}e^{i\omega t}e^{-i\omega' t'}\left\langle \eta_D\left(\vec{x}',t'\right)\eta_D\left(\vec{x},t\right)\right\rangle \\
&= 2D\int d^{SP}xd^{SP}x'dtdt'e^{i\vec{k}\cdot\vec{x}}e^{-i\vec{k}'\cdot\vec{x}'}e^{i\omega t}e^{-i\omega' t'}\delta\left(t-t'\right)\vec{\nabla}\cdot\vec{\nabla}'\left(\bar{c}\left(\vec{x}\right)\delta^{SP}\left(\vec{x}-\vec{x}'\right)\right) \\
&= 2D\left(2\pi\delta\left(\omega-\omega'\right)\right)\int d^{SP}xd^{SP}x'e^{i\vec{k}\cdot\vec{x}}e^{-i\vec{k}'\cdot\vec{x}'}\vec{\nabla}\cdot\vec{\nabla}'\left(\bar{c}\left(\vec{x}\right)\delta^{SP}\left(\vec{x}-\vec{x}'\right)\right) \\
&= 2D\left(2\pi\delta\left(\omega-\omega'\right)\right)\int d^{SP}xd^{SP}x'\bar{c}\left(\vec{x}\right)\delta^{SP}\left(\vec{x}-\vec{x}'\right)\vec{\nabla}\cdot\vec{\nabla}'\left(e^{i\vec{k}\cdot\vec{x}}e^{-i\vec{k}'\cdot\vec{x}'}\right) \\
&= 2D\vec{k}\cdot\vec{k}'\left(2\pi\delta\left(\omega-\omega'\right)\right)\int d^{SP}xd^{SP}x'\bar{c}\left(\vec{x}\right)\delta^{SP}\left(\vec{x}-\vec{x}'\right)e^{i\vec{k}\cdot\vec{x}}e^{-i\vec{k}'\cdot\vec{x}'} \\
&= 2D\vec{k}\cdot\vec{k}'\left(2\pi\delta\left(\omega-\omega'\right)\right)\int d^{SP}x\bar{c}\left(\vec{x}\right)e^{i\vec{x}\left(\vec{k}-\vec{k}'\right)} \\
&= 2D\vec{k}\cdot\vec{k}'\tilde{\bar{c}}\left(\vec{k}-\vec{k}'\right)\left(2\pi\delta\left(\omega-\omega'\right)\right) \\
&= \frac{2\lambda^2\vec{k}\cdot\vec{k}'}{1+\lambda^2\left|\vec{k}-\vec{k}'\right|^2}\left(\beta\left(2\pi\right)^{SO+1}\delta\left(\omega-\omega'\right)\delta^{SO}\left(\vec{k}-\vec{k}'\right)\right).
\end{aligned} \tag{38}$$

Moving on to η_ν, its correlation function must be δ correlated in time and space since it is a purely local reaction and as such, at steady state, must take the form

$$\left\langle \eta_\nu\left(\vec{x}',t'\right)\eta_\nu\left(\vec{x},t\right)\right\rangle = \nu\bar{c}\left(\vec{x}\right)\delta\left(t-t'\right)\delta^{SP}\left(\vec{x}-\vec{x}'\right). \tag{39}$$

Fourier transforming Eq. 39 is again easily performed due to the δ functions and Eq. 24. This yields

$$\begin{aligned}
\left\langle \tilde{\eta}_\nu^*\left(\vec{k}',\omega'\right)\tilde{\eta}_\nu\left(\vec{k},\omega\right)\right\rangle &= \int d^{SP}xd^{SP}x'dtdt'e^{i\vec{k}\cdot\vec{x}}e^{-i\vec{k}'\cdot\vec{x}'}e^{i\omega t}e^{-i\omega' t'}\left\langle \eta_\nu\left(\vec{x}',t'\right)\eta_\nu\left(\vec{x},t\right)\right\rangle \\
&= \nu\int d^{SP}xd^{SP}x'dtdt'e^{i\vec{k}\cdot\vec{x}}e^{-i\vec{k}'\cdot\vec{x}'}e^{i\omega t}e^{-i\omega' t'}\bar{c}\left(\vec{x}\right)\delta\left(t-t'\right)\delta^{SP}\left(\vec{x}-\vec{x}'\right) \\
&= \nu\left(2\pi\delta\left(\omega-\omega'\right)\right)\int d^{SP}xd^{SP}x'e^{i\vec{k}\cdot\vec{x}}e^{-i\vec{k}'\cdot\vec{x}'}\bar{c}\left(\vec{x}\right)\delta^{SP}\left(\vec{x}-\vec{x}'\right) \\
&= \nu\left(2\pi\delta\left(\omega-\omega'\right)\right)\int d^{SP}xe^{i\vec{x}\cdot\left(\vec{k}-\vec{k}'\right)}\bar{c}\left(\vec{x}\right) \\
&= \nu\tilde{\bar{c}}\left(\vec{k}-\vec{k}'\right)\left(2\pi\delta\left(\omega-\omega'\right)\right) \\
&= \frac{1}{1+\lambda^2\left|\vec{k}-\vec{k}'\right|^2}\left(\beta\left(2\pi\right)^{SO+1}\delta\left(\omega-\omega'\right)\delta^{SO}\left(\vec{k}-\vec{k}'\right)\right).
\end{aligned} \tag{40}$$

Finally, the cross spectrum of η_β must be δ correlated in ω-space as well as all source dimensions of k-space since it is merely a uniform production term that does not depend on space or time. This yields

$$\left\langle \tilde{\eta}_\beta^*\left(\vec{k}',\omega'\right)\tilde{\eta}_\beta\left(\vec{k},\omega\right)\right\rangle = \beta\left(2\pi\right)^{SO+1}\delta\left(\omega-\omega'\right)\delta^{SO}\left(\vec{k}-\vec{k}'\right). \tag{41}$$

Combining Eqs. 29, 38, 40, and 41 then yields

$$\left\langle \tilde{\delta c}^{*}\left(\vec{k}',\omega'\right)\tilde{\delta c}\left(\vec{k},\omega\right)\right\rangle = \frac{\beta\left(2\pi\right)^{SO+1}\delta\left(\omega-\omega'\right)\delta^{SO}\left(\vec{k}-\vec{k}'\right)}{\nu^{2}\left(1+\lambda^{2}\left|\vec{k}\right|^{2}-i\frac{\omega}{\nu}\right)\left(1+\lambda^{2}\left|\vec{k}'\right|^{2}+i\frac{\omega'}{\nu}\right)}$$
$$\cdot\left(\frac{2\lambda^{2}\vec{k}\cdot\vec{k}'}{1+\lambda^{2}\left|\vec{k}-\vec{k}'\right|^{2}}+\frac{1}{1+\lambda^{2}\left|\vec{k}-\vec{k}'\right|^{2}}+1\right)$$
$$=\frac{\beta\left(2\pi\right)^{SO+1}\delta\left(\omega-\omega'\right)\delta^{SO}\left(\vec{k}-\vec{k}'\right)}{\nu^{2}\left(1+\lambda^{2}\left|\vec{k}\right|^{2}-i\frac{\omega}{\nu}\right)\left(1+\lambda^{2}\left|\vec{k}'\right|^{2}+i\frac{\omega'}{\nu}\right)}\frac{2+\lambda^{2}\left(\left|\vec{k}\right|^{2}+\left|\vec{k}'\right|^{2}\right)}{1+\lambda^{2}\left|\vec{k}-\vec{k}'\right|^{2}}$$
$$=\frac{\tilde{\tilde{c}}\left(\vec{k}-\vec{k}'\right)\left(2\pi\delta\left(\omega-\omega'\right)\right)\left(2+\lambda^{2}\left(\left|\vec{k}\right|^{2}+\left|\vec{k}'\right|^{2}\right)\right)}{\nu\left(1+\lambda^{2}\left|\vec{k}\right|^{2}-i\frac{\omega}{\nu}\right)\left(1+\lambda^{2}\left|\vec{k}'\right|^{2}+i\frac{\omega'}{\nu}\right)}. \tag{42}$$

We now define m as

$$m\left(\vec{x},t\right)=\int_{V(a)}d^{SP}rc\left(\vec{x}+\vec{r},t\right), \tag{43}$$

where $V\left(a\right)$ is a SP-dimensional sphere with radius a. This allows the mean value of m to be written as

$$\bar{m}\left(\vec{x}\right)=\int_{V(a)}d^{SP}r\bar{c}\left(\vec{x}+\vec{r}\right)=\frac{\beta\lambda^{2-(SP-SO)}}{D}\int_{V(a)}d^{SP}rP_{SP-SO}\left(\frac{\left|\vec{x}+\vec{r}\right|}{\lambda}\right)$$
$$=\frac{\beta\lambda^{SO}}{\nu}M_{SP-SO,SP}\left(\frac{\left|\vec{x}\right|}{\lambda},\frac{a}{\lambda}\right), \tag{44}$$

where

$$M_{N,N'}\left(x,y\right)=\int_{V(y)}d^{N'}uP_{N}\left(\left|\vec{x}+\vec{u}\right|\right). \tag{45}$$

Since $P_{N}\left(\left|\vec{x}\right|\right)$ can only depend on the last N dimensions of its input vectors, the same must be true of $M_{N,N'}$. From here we define $S\left(\vec{x}\right)$ as the 0-frequency limit of the cross spectrum in ω-space of m. This allows the time averaged variance, $\sigma^{2}\left(x\right)$ to take the form

$$
\begin{aligned}
\sigma^2(x) = \frac{S(\vec{x})}{T} &= \frac{1}{T}\lim_{\omega\to 0}\int \frac{d\omega'}{2\pi}\left\langle \delta\tilde{m}^*(\vec{x},\omega')\,\delta\tilde{m}(\vec{x},\omega)\right\rangle \\
&= \frac{1}{T}\lim_{\omega\to 0}\int \frac{d\omega'}{2\pi}\int_{V(a)} d^{SP}r d^{SP}r' \int \frac{d^{SP}k}{(2\pi)^{SP}}\frac{d^{SP}k'}{(2\pi)^{SP}} e^{-i\vec{k}\cdot(\vec{x}+\vec{r})}e^{i\vec{k}'\cdot(\vec{x}+\vec{r}')}\left\langle \tilde{\delta c}^*\left(\vec{k}',\omega'\right)\tilde{\delta c}\left(\vec{k},\omega\right)\right\rangle \\
&= \frac{1}{(2\pi)^{2SP}\nu T}\int_{V(a)} d^{SP}r d^{SP}r' \int d^{SP}k d^{SP}k' e^{-i\vec{k}\cdot(\vec{x}+\vec{r})}e^{i\vec{k}'\cdot(\vec{x}+\vec{r}')} \\
&\quad \cdot \frac{\tilde{\bar{c}}\left(\vec{k}-\vec{k}'\right)\left(2+\lambda^2\left(\left|\vec{k}\right|^2+\left|\vec{k}'\right|^2\right)\right)}{\left(1+\lambda^2\left|\vec{k}\right|^2\right)\left(1+\lambda^2\left|\vec{k}'\right|^2\right)} \\
&= \frac{1}{(2\pi)^{2SP}\nu T}\int_{V(a)} d^{SP}r d^{SP}r' \int d^{SP}k d^{SP}k' d^{SP}z e^{-i\vec{k}\cdot(\vec{x}+\vec{r})}e^{i\vec{k}'\cdot(\vec{x}+\vec{r}')}e^{i\vec{z}\cdot\left(\vec{k}-\vec{k}'\right)} \\
&\quad \cdot \bar{c}(\vec{z})\frac{2+\lambda^2\left(\left|\vec{k}\right|^2+\left|\vec{k}'\right|^2\right)}{\left(1+\lambda^2\left|\vec{k}\right|^2\right)\left(1+\lambda^2\left|\vec{k}'\right|^2\right)} \\
&= \frac{1}{(2\pi)^{2SP}\nu T}\int_{V(a)} d^{SP}r d^{SP}r' \int d^{SP}k d^{SP}k' d^{SP}z e^{-i\vec{k}\cdot(\vec{x}+\vec{r}-\vec{z})}e^{i\vec{k}'\cdot(\vec{x}+\vec{r}'-\vec{z})} \\
&\quad \cdot \bar{c}(\vec{z})\left(\frac{1}{1+\lambda^2\left|\vec{k}\right|^2}+\frac{1}{1+\lambda^2\left|\vec{k}'\right|^2}\right) \\
&= \frac{1}{(2\pi)^{2SP}\nu T}\int_{V(a)} d^{SP}r d^{SP}r' \int d^{SP}z\bar{c}(\vec{z})\left(\int d^{SP}k e^{-i\vec{k}\cdot(\vec{x}+\vec{r}-\vec{z})}\frac{(2\pi)^{SP}\delta^{SP}(\vec{x}+\vec{r}'-\vec{z})}{1+\lambda^2\left|\vec{k}\right|^2}\right. \\
&\quad \left. + \int d^{SP}k' e^{i\vec{k}'\cdot(\vec{x}+\vec{r}'-\vec{z})}\frac{(2\pi)^{SP}\delta^{SP}(\vec{x}+\vec{r}-\vec{z})}{1+\lambda^2\left|\vec{k}'\right|^2}\right) \\
&= \frac{\beta\lambda^{2-(SP-SO)}}{D\nu\lambda^{SP}T}\int_{V(a)} d^{SP}r d^{SP}r' \int d^{SP}z P_{SP-SO}\left(\frac{|\vec{z}|}{\lambda}\right) \\
&\quad \cdot\left(\delta^{SP}(\vec{x}+\vec{r}'-\vec{z})P_{SP}\left(\frac{|\vec{x}+\vec{r}-\vec{z}|}{\lambda}\right)+\delta^{SP}(\vec{x}+\vec{r}-\vec{z})P_{SP}\left(\frac{|\vec{x}+\vec{r}'-\vec{z}|}{\lambda}\right)\right) \\
&= \frac{\beta\lambda^{4-(2SP-SO)}}{D^2T}\int_{V(a)} d^{SP}r d^{SP}r' P_{SP}\left(\frac{|\vec{r}-\vec{r}'|}{\lambda}\right)\left(P_{SP-SO}\left(\frac{|\vec{x}+\vec{r}|}{\lambda}\right)+P_{SP-SO}\left(\frac{|\vec{x}+\vec{r}'|}{\lambda}\right)\right) \\
&= \frac{\beta\lambda^{4-(SP-SO)}}{D^2T}\left(\int_{V(a)} d^{SP}r M_{SP,SP}\left(\frac{|\vec{r}|}{\lambda},\frac{a}{\lambda}\right)P_{SP-SO}\left(\frac{|\vec{x}+\vec{r}|}{\lambda}\right)\right. \\
&\quad \left. + \int_{V(a)} d^{SP}r' M_{SP,SP}\left(\frac{|\vec{r}'|}{\lambda},\frac{a}{\lambda}\right)P_{SP-SO}\left(\frac{|\vec{x}+\vec{r}'|}{\lambda}\right)\right) \\
&= \frac{2\beta\lambda^{4-(SP-SO)}}{D^2T}\int_{V(a)} d^{SP}r M_{SP,SP}\left(\frac{|\vec{r}|}{\lambda},\frac{a}{\lambda}\right)P_{SP-SO}\left(\frac{|\vec{x}+\vec{r}|}{\lambda}\right) \\
&= \frac{2\beta\lambda^{SO}}{\nu^2 T}\Sigma_{SP-SO,SP}\left(\frac{|\vec{x}|}{\lambda},\frac{a}{\lambda}\right) = \frac{2\bar{m}(\vec{x})}{\nu T}\frac{\Sigma_{SP-SO,SP}\left(\frac{|\vec{x}|}{\lambda},\frac{a}{\lambda}\right)}{M_{SP-SO,SP}\left(\frac{|\vec{x}|}{\lambda},\frac{a}{\lambda}\right)},
\end{aligned}
\tag{46}
$$

where

$$\Sigma_{N,N'}(x,y) = \int_{V(y)} d^{N'}u M_{N',N'}(u,y) P_N\left(\left|\vec{x}+\vec{u}\right|\right). \tag{47}$$

Wherein once again only the last N dimensions of the input vectors can be taken into account. Combining Eqs. 44 and 46 yields the full precision to be

$$P^2\left(\vec{x}\right) = \frac{\bar{m}^2\left(\vec{x}\right)}{\sigma^2\left(\vec{x}\right)}\left(\frac{\Delta\bar{m}\left(\vec{x}\right)}{\bar{m}\left(\vec{x}\right)}\right)^2 = \frac{T}{2\tau}\frac{\beta}{\nu}M_{SP-SO,SP}\left(\frac{\left|\vec{x}\right|}{\lambda},\frac{a}{\lambda}\right)\left(1-\frac{M_{SP-SO,SP}\left(\frac{\left|\vec{x}\right|+2a}{\lambda},\frac{a}{\lambda}\right)}{M_{SP-SO,SP}\left(\frac{\left|\vec{x}\right|}{\lambda},\frac{a}{\lambda}\right)}\right)^2, \tag{48}$$

where

$$\tau = \frac{1}{\nu}\frac{\Sigma_{SP-SO,SP}\left(\frac{\left|\vec{x}\right|}{\lambda},\frac{a}{\lambda}\right)}{M_{SP-SO,SP}\left(\frac{\left|\vec{x}\right|}{\lambda},\frac{a}{\lambda}\right)}. \tag{49}$$

With Eq. 48, once the forms of P_N, $M_{N,N'}$, and $\Sigma_{N,N'}$ are determined for a given SP and SO, the full form of the noise-to-signal ratio can be found. We now calculate these forms for specific choices of SP and SO.

1D space, 0D source

To begin, we start with the simple scenario in which $SP = 1$ and $SO = 0$. This allows P_1, $M_{1,1}$, and $\Sigma_{1,1}$ to take the forms

$$P_1(x) = \int \frac{du}{2\pi}e^{-iux}\frac{1}{1+u^2} = \frac{1}{2}e^{-|x|} \tag{50}$$

$$\begin{aligned} M_{1,1}(x,y) &= \int_{-y}^{y} du P_1\left(|x+u|\right) = \frac{1}{2}\int_{-y}^{y} du e^{-|x+u|} \\ &= \begin{cases} 1-e^{-y}\cosh(x) & x < y \\ e^{-x}\sinh(y) & x \geq y \end{cases} \end{aligned} \tag{51}$$

$$\begin{aligned} \Sigma_{1,1}(x,y) &= \int_{-y}^{y} du M_{1,1}(u,y) P_1\left(|x+u|\right) = \frac{1}{2}\int_{-y}^{y} du\left(1-e^{-y}\cosh(u)\right)e^{-|x+u|} \\ &= \begin{cases} 1-\frac{1}{4}e^{-y}\left(\left(5+2y-e^{-2y}\right)\cosh(x)-2x\sinh(x)\right) & x < y \\ \frac{1}{4}e^{-x}\left(4\sinh(y)-e^{-y}\left(2y+\sinh\left(2y\right)\right)\right) & x \geq y \end{cases}. \end{aligned} \tag{52}$$

Eqs. 51 and 52 can then be put into Eq. 48 along with the assumption $|x| > a$ to obtain

$$P^2(x) = \frac{\bar{m}(x)T}{2\tau}\left(1-e^{-\frac{2a}{\lambda}}\right)^2, \tag{53}$$

and

$$\tau = \frac{1}{\nu}\left(1-e^{-\frac{a}{\lambda}}\frac{\frac{2a}{\lambda}+\sinh\left(\frac{2a}{\lambda}\right)}{4\sinh\left(\frac{a}{\lambda}\right)}\right) \tag{54}$$

as in Eqs. 9 and 10 of the main text.

Next we apply the condition given by Eq. 17 to determine the regime in which these results are valid for the $SP = 1$ and $SO = 0$ case. A similar methodology can be done for each of the other

cases we will look at, though this is the only one we do explicitly. To begin, we will reperform the calculation done in Eq. 46 but without taking the $\omega \to 0$ limit so as to obtain the full form of $S(\omega, x)$.

$$\begin{aligned}
S(\omega,x) &= \int \frac{d\omega'}{2\pi} \left\langle \delta\tilde{m}^*(x,\omega')\, \delta\tilde{m}(x,\omega) \right\rangle \\
&= \int \frac{d\omega'}{2\pi} \int_{-a}^{a} dr dr' \int \frac{dk}{2\pi}\frac{dk'}{2\pi} e^{-ik(x+r)} e^{ik'(x+r')} \left\langle \delta\tilde{c}^*(k',\omega')\, \delta\tilde{c}(k,\omega) \right\rangle \\
&= \frac{1}{(2\pi)^2 \nu} \int_{-a}^{a} dr dr' \int dk dk' e^{-ik(x+r)} e^{ik'(x+r')} \frac{\tilde{\bar{c}}(k-k') \left(2+\lambda^2\left(k^2+k'^2\right)\right)}{\left(1+\lambda^2 k^2 - i\frac{\omega}{\nu}\right)\left(1+\lambda^2 k'^2 + i\frac{\omega}{\nu}\right)} \\
&= \frac{1}{(2\pi)^2 \nu} \int_{-a}^{a} dr dr' \int dk dk' dz e^{-ik(x+r)} e^{ik'(x+r')} e^{iz(k-k')} \bar{c}(z) \frac{2+\lambda^2\left(k^2+k'^2\right)}{\left(1+\lambda^2 k^2 - i\frac{\omega}{\nu}\right)\left(1+\lambda^2 k'^2 + i\frac{\omega}{\nu}\right)} \\
&= \frac{1}{(2\pi)^2 \nu} \int_{-a}^{a} dr dr' \int dk dk' dz e^{-ik(x+r-z)} e^{ik'(x+r'-z)} \bar{c}(z) \left(\frac{1}{1+\lambda^2 k^2 - i\frac{\omega}{\nu}} + \frac{1}{1+\lambda^2 k'^2 + i\frac{\omega}{\nu}} \right) \\
&= \frac{1}{(2\pi)^2 \nu} \int_{-a}^{a} dr dr' \int dz \bar{c}(z) \left(\int dk e^{-ik(x+r-z)} \frac{2\pi\delta(x+r'-z)}{1+\lambda^2 k^2 - i\frac{\omega}{\nu}} + \int dk' e^{ik'(x+r'-z)} \frac{2\pi\delta(x+r-z)}{1+\lambda^2 k'^2 + i\frac{\omega}{\nu}} \right) \\
&= \frac{1}{2\pi\nu} \int_{-a}^{a} dr dr' \left(\int dk e^{-ik(r-r')} \frac{\bar{c}(x+r')}{1+\lambda^2 k^2 - i\frac{\omega}{\nu}} + \int dk e^{ik(r'-r)} \frac{\bar{c}(x+r)}{1+\lambda^2 k^2 + i\frac{\omega}{\nu}} \right) \\
&= \frac{1}{\nu\lambda} \int_{-a}^{a} dr dr' \left(\bar{c}(x+r') Q\left(\frac{r-r'}{\lambda}, -\frac{\omega}{\nu}\right) + \bar{c}(x+r) Q\left(\frac{r-r'}{\lambda}, \frac{\omega}{\nu}\right) \right),
\end{aligned} \tag{55}$$

where

$$Q(x,y) = \int \frac{du}{2\pi} e^{-iux} \frac{1}{1+iy+u^2} = \frac{1}{2\sqrt{1+iy}} e^{-|x|\sqrt{1+iy}} \tag{56}$$

and $\sqrt{1+iy}$ is assumed to be the branch with a positive real component. Plugging this and the explicit form of $\bar{c}$ into Eq. 55 then yields

$$\begin{aligned}
S(\omega,x) &= \frac{\beta}{4\nu D} \int_{-a}^{a} dr dr' \left(\frac{1}{\sqrt{1-i\frac{\omega}{\nu}}} e^{-\frac{|x+r'|}{\lambda}} e^{-\frac{|r-r'|}{\lambda}\sqrt{1-i\frac{\omega}{\nu}}} + \frac{1}{\sqrt{1+i\frac{\omega}{\nu}}} e^{-\frac{|x+r|}{\lambda}} e^{-\frac{|r-r'|}{\lambda}\sqrt{1+i\frac{\omega}{\nu}}} \right) \\
&= \frac{\beta}{2\nu D} \mathrm{Re}\left[\int_{-a}^{a} dr dr' \frac{1}{\sqrt{1+i\frac{\omega}{\nu}}} e^{-\frac{|x+r|}{\lambda}} e^{-\frac{|r-r'|}{\lambda}\sqrt{1+i\frac{\omega}{\nu}}} \right] = \frac{2\beta}{\nu^2} \mathrm{Re}\left[\Upsilon\left(\frac{|x|}{\lambda}, \frac{a}{\lambda}, \sqrt{1+i\frac{\omega}{\nu}}\right) \right],
\end{aligned} \tag{57}$$

where

$$\Upsilon(x,y,w) = \int_{-y}^{y} du du' \frac{1}{4w} e^{-|x+u|} e^{-u|u-u'|}. \tag{58}$$

The function $\Upsilon(x,y,w)$ limits to $\Sigma_{1,1}(x,y)$ when $w \to 1$ and as such has different forms when x is less or greater than y. As the purpose of this exercise is to determine the regime in which our theoretical approximations are valid and our model obeys $|x| \geq 2a$ for all cells, here we will only present the $x > y$ solution for simplicity. Using this to perform the integrals in Eq. 58 and applying the result to Eq. 57 then yields

$$S(\omega,x) = \frac{2\beta}{\nu^2} e^{-\frac{|x|}{\lambda}} \mathrm{Re}\left[\frac{1}{W^2} \sinh\left(\frac{a}{\lambda}\right) - e^{-\frac{a}{\lambda}W} \frac{W \sinh\left(\frac{a}{\lambda}W\right)\cosh\left(\frac{a}{\lambda}\right) - \cosh\left(\frac{a}{\lambda}W\right)\sinh\left(\frac{a}{\lambda}\right)}{W^2\left(W^2-1\right)} \right], \tag{59}$$

where $W = \sqrt{1 + i\frac{\omega}{\nu}}$, which in turn implies $\omega = -i\nu(W^2 - 1)$. With this, it is easier to perform all further calculations with respect to W and take the $W \to 1$ limit as that is equivalent to the $\omega \to 0$ limit.

We can now combine this with the known form of $S(0, x)$ given in Eq. 46 to evaluate Eq. 17 to take the form

$$\begin{aligned} T^2 \gg \left| \frac{6}{S}\frac{\partial^2 S}{\partial \omega^2}\bigg|_{\omega=0} \right| &= \left| \frac{6}{S}\frac{\partial W}{\partial \omega}\frac{\partial}{\partial W}\left(\frac{\partial W}{\partial \omega}\frac{\partial S}{\partial W}\right)\bigg|_{W=1} \right| = \left| \frac{6}{S}\left(\left(\frac{\partial \omega}{\partial W}\right)^{-2}\frac{\partial^2 S}{\partial W^2} - \left(\frac{\partial \omega}{\partial W}\right)^{-3}\frac{\partial^2 \omega}{\partial W^2}\frac{\partial S}{\partial W}\right)\bigg|_{W=1} \right| \\ &= \frac{1}{2\nu^2}\frac{96\sinh\left(\frac{a}{\lambda}\right) - e^{-\frac{a}{\lambda}}\left(48\frac{a}{\lambda} + 30\left(\frac{a}{\lambda}\right)^2 + 8\left(\frac{a}{\lambda}\right)^3 + 33\sinh\left(2\frac{a}{\lambda}\right)\right) + 6e^{-3\frac{a}{\lambda}}\left(3\frac{a}{\lambda} + \left(\frac{a}{\lambda}\right)^2\right)}{4\sinh\left(\frac{a}{\lambda}\right) - e^{-\frac{a}{\lambda}}\left(2\frac{a}{\lambda} + \sinh\left(2\frac{a}{\lambda}\right)\right)}. \end{aligned} \tag{60}$$

The right-hand side of Eq. 60 is a function that monotonically increases from $9/2\nu^2$ to $21/2\nu^2$ as a/λ goes from 0 to ∞. Thus, regardless of the value of λ, ν sets the timescale to which T must be compared.

2D space, 0D source

For $SP = 2$ and $SO = 0$, P_2, $M_{2,2}$, and $\Sigma_{2,2}$ each take the form

$$P_2(x) = \int \frac{d^2u}{(2\pi)^2} e^{-i\vec{u}\cdot\vec{x}} \frac{1}{1 + |\vec{u}|^2} = \frac{1}{2\pi} K_0(x) \tag{61}$$

$$\begin{aligned} M_{2,2}(x, y) = \int_{V(y)} d^2u P_2\left(|\vec{x} + \vec{u}|\right) &= \int_{V(y)} d^2u \int \frac{d^2u'}{(2\pi)^2} e^{-i\vec{u}'\cdot(\vec{x}+\vec{u})} \frac{1}{1 + |\vec{u}'|^2} \\ &= y\int_0^\infty du' \frac{J_0(xu')\,J_1(yu')}{1 + u'^2} \end{aligned} \tag{62}$$

$$\begin{aligned} \Sigma_{2,2}(x, y) &= \int_{V(y)} d^2u M_{2,2}\left(|\vec{u}|, y\right) P_2\left(|\vec{x} + \vec{u}|\right) \\ &= y\int_{V(y)} d^2u \int_0^\infty du' \int \frac{d^2u''}{(2\pi)^2} \frac{J_0\left(|\vec{u}|\,u'\right) J_1(yu')}{1 + u'^2} \frac{e^{-i\vec{u}''\cdot(\vec{x}+\vec{u})}}{1 + |\vec{u}''|^2} \\ &= y^2\int_0^\infty du'du'' \frac{u''J_0(xu'')\,J_1(yu')\left(u'J_0(yu'')\,J_1(yu') - u''J_0(yu')\,J_1(yu'')\right)}{\left(u'^2 - u''^2\right)\left(1 + u'^2\right)\left(1 + u''^2\right)}, \end{aligned} \tag{63}$$

where $J_n(x)$ and $K_n(x)$ are the Bessel functions of the first kind and modified Bessel functions of the second kind respectively. Unfortunately, the complicated nature of Bessel functions makes the remaining integrals unsolvable analytically, and therefore we evaluate them numerically. Similar problems arise whenever $SP = 2$ or $SP - SO = 2$.

3D space, 0D source

For $SP = 3$ and $SO = 0$, P_3, $M_{3,3}$, and $\Sigma_{3,3}$ each take the form

$$P_3(x) = \int \frac{d^3u}{(2\pi)^3} e^{-i\vec{u}\cdot\vec{x}} \frac{1}{1 + |\vec{u}|^2} = \frac{1}{4\pi x} e^{-x} \tag{64}$$

$$\begin{aligned} M_{3,3}(x, y) = \int_{V(y)} d^3u P_3\left(|\vec{x} + \vec{u}|\right) &= \frac{1}{4\pi}\int_{V(y)} d^3u \frac{1}{|\vec{x} + \vec{u}|} e^{-|\vec{x}+\vec{u}|} \\ &= \begin{cases} 1 - \frac{1+y}{x}e^{-y}\sinh(x) & x < y \\ \frac{1}{x}e^{-x}\left(y\cosh(y) - \sinh(y)\right) & x \geq y \end{cases} \end{aligned} \tag{65}$$

$$\begin{aligned}\Sigma_{3,3}(x,y) &= \int_{V(y)} d^3u M_{3,3}\left(|\vec{u}|,y\right) P_3\left(|\vec{x}+\vec{u}|\right) \\ &= \frac{1}{4\pi}\int_{V(y)} d^3u\left(1-\frac{1+y}{|\vec{u}|}e^{-y}\sinh\left(|\vec{u}|\right)\right)\frac{1}{|\vec{x}+\vec{u}|}e^{-|\vec{x}+\vec{u}|} \\ &= \begin{cases} 1-\frac{1}{4x}e^{-y}\left(1+y\right)\left(\left(5+2y+e^{-2y}\right)\sinh(x)-2x\cosh(x)\right) & x<y \\ \frac{1}{4x}e^{-x}\left(4\left(y\cosh(y)-\sinh(y)\right)+e^{-y}\left(1+y\right)\left(2y-\sinh\left(2y\right)\right)\right) & x\geq y \end{cases}\end{aligned} \tag{66}$$

2D space, 1D source

For $SP=2$, $SO=1$, P_1 and $M_{2,2}$ are known from Eqs. 50 and 62. This leaves $M_{1,2}$ and $\Sigma_{1,2}$ to take the forms

$$\begin{aligned}M_{1,2}(x,y) &= \int_{V(y)} d^2u P_1\left(|\vec{x}+\vec{u}|\right) = \frac{1}{2}\int_0^y du\int_0^{2\pi} d\theta u e^{-|x_2+u_2|} \\ &= e^{-|x_2|}\int_0^{2\pi} d\theta\frac{1-e^{-y\sin(\theta)}\left(1+y\sin(\theta)\right)}{2\left(\sin(\theta)\right)^2}\end{aligned} \tag{67}$$

$$\Sigma_{1,2}(x,y) = \int_{V(y)} d^2u M_{2,2}\left(|\vec{u}|,y\right) P_1\left(|\vec{x}+\vec{u}|\right) = \frac{y}{2}\int_0^y du\int_0^{2\pi} d\theta\int_0^{\infty} du' u\frac{J_0\left(uu'\right)J_1\left(yu'\right)}{1+u'^2}e^{-|x_2+u\sin(\theta)|} \tag{68}$$

Again, we evaluate the remaining integrals numerically.

3D space, 2D source

For $SP=3$, $SO=2$, P_1 and $M_{3,3}$ are known from Eqs. 50 and 65. This leaves $M_{1,3}$ and $\Sigma_{1,3}$ to take the forms

$$\begin{aligned}M_{1,3}(x,y) &= \int_{V(y)} d^3u P_1\left(|\vec{x}+\vec{u}|\right) = \frac{1}{2}\int_{V(y)} d^3u e^{-|x_3+u_3|} \\ &= 2\pi\begin{cases} e^{-y}\left(1+y\right)\cosh(x)+\frac{y^2-x^2}{2}-1 & x<y \\ e^{-x}\left(y\cosh(y)-\sinh(y)\right) & x\geq y \end{cases}\end{aligned} \tag{69}$$

$$\begin{aligned}\Sigma_{1,3}(x,y) &= \int_{V(y)} d^3u M_{3,3}\left(|\vec{u}|,y\right) P_1\left(|\vec{x}+\vec{u}|\right) = \frac{1}{2}\int_{V(y)} d^3u\left(1-\frac{1+y}{|\vec{u}|}e^{-y}\sinh\left(|\vec{u}|\right)\right)e^{-|x_3+u_3|} \\ &= 2\pi\begin{cases} e^{-y}\left(1+y\right)\left(\frac{7+2y+e^{-2y}}{4}\cosh(x)-\frac{x}{2}\sinh(x)-\cosh(y)\right)+\frac{y^2-x^2}{2}-1 & x<y \\ e^{-x}\left(\frac{4y^2+5y-1}{8}e^{-y}+\frac{1+y}{8}e^{-3y}+\frac{3y}{4}\cosh(y)-\frac{5}{4}\sinh(y)\right) & x\geq y \end{cases}\end{aligned} \tag{70}$$

Appendix 2: Hopping model for SDC case

To obtain a more intuitive understanding of why the SDC model results in the scaling properties seen in the various calculations of $M_{\text{SP-SO,SP}}$ and $\Sigma_{\text{SP-SO,SP}}$, we now look at a simpler version of one dimensional diffusion in which we discretize space into compartments of uniform size. Let molecules still be produced in the 0th compartment at rate β and degrade anywhere in space at rate ν. The process of diffusion can be approximated by letting the molecules hop to neighboring compartments with rate h with equal probability of moving left or right. This allows the dynamics of m_j, the number of molecules in the j compartment for $j\in\mathbb{Z}$, to be written as

$$\frac{\partial m_j}{\partial t} = \beta\delta_{0j} + h\left(m_{j+1}+m_{j-1}-2m_j\right) - \nu m_j. \tag{71}$$

By setting the left-hand side of Eq. 71 to 0, the resulting system of equations can be easily solved by assuming $\bar{m}_j = A\exp(-2|j|/\lambda)$ and calculating A and λ. Imposing this assumption on Eq. 71 and taking $j > 0$ yields

$$\begin{aligned} 0 &= h\left(Ae^{-\frac{2(j+1)}{\lambda}} + Ae^{-\frac{2(j-1)}{\lambda}} - 2Ae^{-\frac{2j}{\lambda}}\right) - \nu Ae^{-\frac{2j}{\lambda}} = Ae^{-\frac{2j}{\lambda}}\left(he^{-\frac{2}{\lambda}} + he^{\frac{2}{\lambda}} - 2h - \nu\right) \\ &= Ae^{-\frac{2j}{\lambda}}\left(4h\sinh^2\left(\frac{1}{\lambda}\right) - \nu\right) \implies \lambda = \operatorname{asinh}^{-1}\left(\sqrt{\frac{\nu}{4h}}\right). \end{aligned} \tag{72}$$

With λ solved for, we solve for the proportionality constant by noting that the total number of molecules in the whole system must follow a simple birth-death process with a mean of β/ν. This in turn implies

$$\begin{aligned} \frac{\beta}{\nu} &= \sum_{j=-\infty}^{\infty} Ae^{-\frac{2|j|}{\lambda}} = A\left(2\left(\sum_{j=0}^{\infty} e^{-\frac{2j}{\lambda}}\right) - 1\right) = A\left(\frac{2}{1-e^{-\frac{2}{\lambda}}} - 1\right) = A\left(\frac{e^{\frac{1}{\lambda}}}{\sinh\left(\frac{1}{\lambda}\right)} - 1\right) = A\coth\left(\frac{1}{\lambda}\right) \\ &\implies A = \frac{\beta}{\nu}\tanh\left(\frac{1}{\lambda}\right), \end{aligned} \tag{73}$$

This in turn gives the average value of m_j to be

$$\bar{m}_j = \frac{\beta}{\nu}\tanh\left(\frac{1}{\lambda}\right)e^{-\frac{2|j|}{\lambda}}. \tag{74}$$

Next, we calculate the full distribution of m_j by assuming that at any given moment in time each molecule in the system has probability P_j of being in the jth compartment. This can be combined with the aforementioned fact that N, the total number of molecules in the system, must follow a birth-death process and thus to Poissonianly distributed with mean β/ν. For any given value of N, $P(m_j|N)$ must be a binomial distribution with success probability P_j since each molecule is independent. This allows the marginal distribution $P(m_j)$ to be calculated to be

$$\begin{aligned} P\left(m_j\right) &= \sum_{N=m_j}^{\infty} P\left(N\right)P\left(m_j|N\right) = \sum_{N=m_j}^{\infty} e^{-\frac{\beta}{\nu}}\frac{\left(\frac{\beta}{\nu}\right)^N}{N!}\binom{N}{m_j}P_j^{m_j}\left(1-P_j\right)^{N-m_j} \\ &= e^{-\frac{\beta}{\nu}}\frac{\left(\frac{\beta}{\nu}P_j\right)^{m_j}}{m_j!}\sum_{N=m_j}^{\infty}\frac{\left(\frac{\beta}{\nu}\left(1-P_j\right)\right)^{N-m_j}}{\left(N-m_j\right)!} = e^{-\frac{\beta}{\nu}}\frac{\left(\frac{\beta}{\nu}P_j\right)^{m_j}}{m_j!}e^{\frac{\beta}{\nu}\left(1-P_j\right)} = e^{-\frac{\beta}{\nu}P_j}\frac{\left(\frac{\beta}{\nu}P_j\right)^{m_j}}{m_j!}. \end{aligned} \tag{75}$$

Thus, m_j is seen to be Poissonianly distributed with mean $\beta P_j/\nu$. Comparing this mean to that derived in Eq. 74 then implies

$$P_j = \tanh\left(\frac{1}{\lambda}\right)e^{-\frac{2|j|}{\lambda}}. \tag{76}$$

We now consider the joint distribution of m_j and m_k for $j \neq k$. Since molecules cannot be in the jth and kth compartment simultaneously, the joint conditional distribution $P(m_j, m_k|N)$ must be trinomially distributed. This allows for the joint distribution to be calculated in a manner similar to Eq. 75 to produce

$$P\left(m_j, m_k\right) = \sum_{N=m_j+m_k}^{\infty} P\left(N\right) P\left(m_j, m_k | N\right) = \sum_{N=m_j+m_k}^{\infty} e^{-\frac{\beta}{\nu}} \frac{\left(\frac{\beta}{\nu}\right)^N}{N!} \binom{N}{m_j, m_k} P_j^{m_j} P_k^{m_k} \left(1 - P_j - P_k\right)^{N-m_j-m_k}$$
$$= e^{-\frac{\beta}{\nu}} \frac{\left(\frac{\beta}{\nu} P_j\right)^{m_j}}{m_j!} \frac{\left(\frac{\beta}{\nu} P_k\right)^{m_k}}{m_k!} \sum_{N=m_j+m_k}^{\infty} \frac{\left(\frac{\beta}{\nu}\left(1 - P_j - P_k\right)\right)^{N-m_j-m_k}}{\left(N - m_j - m_k\right)!}$$
$$= e^{-\frac{\beta}{\nu}} \frac{\left(\frac{\beta}{\nu} P_j\right)^{m_j}}{m_j!} \frac{\left(\frac{\beta}{\nu} P_k\right)^{m_k}}{m_k!} e^{\frac{\beta}{\nu}\left(1-P_j-P_k\right)} = \left(e^{-\frac{\beta}{\nu} P_j} \frac{\left(\frac{\beta}{\nu} P_j\right)^{m_j}}{m_j!}\right)\left(e^{-\frac{\beta}{\nu} P_k} \frac{\left(\frac{\beta}{\nu} P_k\right)^{m_k}}{m_k!}\right). \tag{77}$$

Thus the joint probability distribution of m_j and m_k is seen to be separable into the product of the two marginal distribution, meaning that same-time, instantaneous measurements of m_j an m_k must be uncorrelated.

From here we can begin to calculate the full correlation function for m_j and m_k. We start by defining $\delta m_j(t) = m_j(t) - \bar{m}_j$ and $\delta m_k(t) = m_k(t) - \bar{m}_k$. Since $\bar{m}_j$ is known to set the right-hand side of Eq. 71 to 0, the dynamics of δm_j can be written as

$$\frac{\partial \delta m_j}{\partial t} = h\left(\delta m_{j+1} + \delta m_{j-1} - 2\delta m_j\right) - \nu \delta m_j, \tag{78}$$

with the same being true for δm_k. Additionally, we assume the system is at steady state so that all mean expressions are invariant to time translation. Given this, we can without loss of generality take the correlation function between δm_j and δm_k to have the form

$$C_{j,k}\left(t\right) = \left\langle \delta m_k\left(t\right) \delta m_j\left(0\right) \right\rangle, \tag{79}$$

where $t > 0$. Applying the dynamic result given in Eq. 78 then yields

$$\frac{\partial C_{j,k}}{\partial t} = \left\langle \frac{\partial \delta m_k(t)}{\partial t} \delta m_j(0) \right\rangle = \left\langle \left(h\left(\delta m_{k+1}(t) + \delta m_{k-1}(t) - 2\delta m_k(t)\right) - \nu \delta m_k(t)\right) \delta m_j\left(0\right) \right\rangle$$
$$= h\left(C_{j,k+1} + C_{j,k-1}\right) - \left(2h + \nu\right) C_{j,k}. \tag{80}$$

The final form of Eq. 80 can be split into the term $-(2h+\nu)C_{j,k}$ which implies $C_{j,k} \propto \exp(-(2h+\nu)t)$ and the term $h(C_{j,k+1} + C_{j,k-1})$ which is the recursion relation for $I_\ell(2ht)$, the modified Bessel function of the first kind, where ℓ is some function of j and k. This means $C_{j,k}(t)$ can be written as

$$C_{j,k}\left(t\right) = A I_{\ell(j,k)}\left(2ht\right) e^{-(2h+\nu)t}, \tag{81}$$

for some proportionality constant A.

To determine the forms of A and $\ell(j,k)$, we can utilize the initial condition that m_j is Poissonianlly distributed and thus has a variance equal to its mean while being completely uncorrelated with m_k when both are measured at the same time. This means $C_{j,k}(0)$ can be written as

$$C_{j,k}\left(0\right) = \frac{\beta}{\nu} P_j \delta_{jk}, \tag{82}$$

which in turn implies $\ell(j,j) = 0$ as $I_n(0) = \delta_{0n}$ for $n \in \mathbb{Z}$. To satisfy the recursion relation term of Eq. 80, it must then be the case that $\ell(j, j+n) = n$. Setting $k = j + n$ thus yields $\ell(j,k) = k - j$. Since k and j are integers, $\ell(j,k) = j - k$ is equally valid as $I_n = I_{-n}$ again for $n \in \mathbb{Z}$. Combining these results together yields the final form of $C_{j,k}(t)$ to be

$$C_{j,k}\left(t\right) = \frac{\beta}{\nu} P_j I_{k-j}\left(2ht\right) e^{-(2h+\nu)t}. \tag{83}$$

Next, let τ be the autocorrelation time of m_j. This quantity is typically defined by integrating $C_{j,j}(t)/C_{j,j}(0)$ over all time. Using the known properties of modified Bessel functions, this can be solved to yield

$$\tau = \int_0^\infty dt \frac{C_{j,j}(t)}{C_{j,j}(0)} = \int_0^\infty dt\, I_0\left(2ht\right) e^{-(2h+\nu)t} = \frac{1}{\sqrt{\nu\left(4h+\nu\right)}}. \tag{84}$$

If we now define $M = T/\tau$ where M is the number of effectively independent measurements that can be made in a time T, we see that for $h \gg \nu$, $M \approx 2\sqrt{\nu h}T$. Additionally, from Eq. 72 we see that in the $h \gg \nu$ regime $\lambda \approx 2\sqrt{h/\nu}$. By equating this λ to the nondimensionalized λ_{SDC}/a from the SDC model we see that $M \approx \lambda\nu T = (\lambda_{\text{SDC}}/a)\nu T$. This is consistent with the fact that for $\lambda_{\text{SDC}} \gg a$ the right-hand side of Eq. 54 becomes approximately $a/\lambda_{\text{SDC}}\nu$, which allows $M = T/\tau_{SDC} \approx \left(\lambda_{\text{SDC}}/a\right)\nu T$.

In the $h \ll \nu$ regime we find $M \approx \nu T$. Once again, this consistent with Eq. 54 when $\lambda_{\text{SDC}} \ll a$ as this causes the right-hand side to become approximately ν^{-1}. Thus, the SDC model is seen to have a correlation time that agrees with Eq. 84 in both the large and small h regime.

Appendix 3: Comparison to experimental data

To compare our theory to experimental data, we focus on ten of the morphogens presented in Table 1 of ***Kicheva et al.*** (***2012***) and obtain data from the references therein. For Bicoid, we obtain a value of λ of ~100μm from the text of ***Gregor et al.*** (***2007b***) with and error of $\pm$10μm from the finding in ***Gregor et al.*** (***2007a***) that cells have a ~10% error in measuring the Bicoid gradient. We then take the a value of the *Drosophila* embryo cells that are subjected to the Bicoid gradient to be ~2.8μm based on Fig. 3A of ***Gregor et al.*** (***2007a***). We use the same figure to estimate the size of the whole embryo to be ~500μm or ~90 cells. This value of a is also used for Dorsal as measurements of both Bicoid and Dorsal occur in the *Drosophila* embryo at nuclear cycle 14. For the value of λ for Dorsal, we use Fig. 3D from ***Liberman et al.*** (***2009***) to obtain a full width at 60% max of 45$\pm$10μm. Since this represents the width of Gaussian fit on both sides of the source whereas our model uses an exponential profile, we assume the appropriate λ value for such an exponential fit would be half this value, 22.5$\pm$5μm. Fig. 3A from the same source also shows that the distance from the ventral midline to the dorsal midline is ~200μm or ~35 cells.

For Dpp and Wg, ***Kicheva et al.*** (***2007***) provides explicit measurements of λ for each. These values are 20.2$\pm$5.7μm and 5.8$\pm$2.04μm respectively. For Hh, we use Fig. S2C in the supplementary material of ***Wartlick et al.*** (***2011***) to determine λ to be 8$\pm$3μm. Dpp, Wg, and Hh all occur in the wing disc during the third instar of the *Drosophila* development. As such, we use a common value of a for all three. This value is taken to be 1.3μm based on the area of the cells being reported as 5.5$\pm$0.8μm^2 in the supplementary material of ***Kicheva et al.*** (***2007***) and the assumption that the cells are circular. Additionally, the scale bar for Fig. 1A in ***Wartlick et al.*** (***2011***) shows the maximal distance from the morphogen producing midline of the wing disc to its edge to be ~250μm or ~100 cells.

The λ value of Fgf8 is reported as being 197$\pm$7μm in ***Yu et al.*** (***2009***). Additionally, based off the scale bars seen in Fig. 2C-E of ***Yu et al.*** (***2009***), we estimate the value of a for the cells to be ~10μm. For the morphogens involved in the Nodal/Lefty system (cyclops, squint, lefty1, and lefty2), measurements of λ for each are taken from Fig. 2C-F of ***Müller et al.*** (***2012***) by observing where the average of the three curves crosses the 37% of max threshold with error bars given by the width of the region in which the vertical error bars of each plot intersect this threshold line. We assume the a value of each morphogen in the Nodal/Lefty system to be equivalent to the a value of cells in the Fgf8 measurements performed in ***Yu et al.*** (***2009***). This is because the measurements made in ***Müller et al.*** (***2012***) were taken during the blastula stage of the zebrafish development while measurements taken in ***Yu et al.*** (***2009***) we taken in the sphere germ ring stage. These stages occur at ~2.25 and ~5.67 hpf respectively, but the blastula stage can last until ~6 hpf based on the timeline of zebrafish development presented in ***Kimmel et al.*** (***1995***). As such, since there is

potential overlap in the time frame of these two stages, we assume the cells maintain a relatively fixed size and thus that the value of a for the Nodal/Lefty system can be taken as the same value of a used for Fgf8. Additionally, as seen in Figs. 8F and 11B in ***Kimmel et al.*** (***1995***), these two stages also share a rougly equal overall diameter of the embryo of ∼500μm at the largest point. This creates a circumference of ∼1600μm or ∼80 cells, which in turn means the morphogen must travel a maximum distance of ∼40 cells away from the source.

Morphogen	Organism	λ (μm)	a (μm)	N
Bicoid	*Drosophila*	100±10	2.8	90
Fgf8	Zebrafish	197±7	10	40
Lefty2	Zebrafish	150±25	10	40
Lefty1	Zebrafish	115±20	10	40
Dpp	*Drosophila*	20.2±5.7	1.3	100
Dorsal	*Drosophila*	22.5±5	2.8	35
Squint	Zebrafish	65±10	10	40
Cyclops	Zebrafish	30±5	10	40
Hh	*Drosophila*	8±3	1.3	100
Wg	*Drosophila*	5.8±2.04	1.3	100

References

Akiyama T, Gibson MC. Morphogen transport: theoretical and experimental controversies. Wiley Interdisciplinary Reviews: Developmental Biology. 2015; 4(2):99–112.

Berezhkovskii AM, Sample C, Shvartsman SY. Formation of morphogen gradients: Local accumulation time. Physical Review E. 2011; 83(5):051906.

Berg HC, Purcell EM. Physics of chemoreception. Biophysical journal. 1977; 20(2):193–219.

Bischoff M, Gradilla AC, Seijo I, Andrés G, Rodríguez-Navas C, González-Méndez L, Guerrero I. Cytonemes are required for the establishment of a normal Hedgehog morphogen gradient in Drosophila epithelia. Nature cell biology. 2013; 15(11):1269.

Bressloff PC, Kim H. Bidirectional transport model of morphogen gradient formation via cytonemes. Physical biology. 2018; .

Carrell SN, O'Connell MD, Jacobsen T, Pomeroy AE, Hayes SM, Reeves GT. A facilitated diffusion mechanism establishes the Drosophila Dorsal gradient. Development. 2017; 144(23):4450–4461.

Chen W, Huang H, Hatori R, Kornberg TB. Essential basal cytonemes take up Hedgehog in the Drosophila wing imaginal disc. Development. 2017; 144(17):3134–3144.

De Lachapelle AM, Bergmann S. Precision and scaling in morphogen gradient read-out. Molecular systems biology. 2010; 6(1):351.

Driever W, Nüsslein-Volhard C. The bicoid protein determines position in the Drosophila embryo in a concentration-dependent manner. Cell. 1988; 54(1):95–104.

Dubuis JO, Tkačik G, Wieschaus EF, Gregor T, Bialek W. Positional information, in bits. Proceedings of the National Academy of Sciences. 2013; 110(41):16301–16308.

Ellery AJ, Simpson MJ, McCue SW, Baker RE. Characterizing transport through a crowded environment with different obstacle sizes. The Journal of chemical physics. 2014; 140(5):02B601_1.

Erdmann T, Howard M, Ten Wolde PR. Role of spatial averaging in the precision of gene expression patterns. Physical review letters. 2009; 103(25):258101.

Fancher S, Mugler A. Fundamental limits to collective concentration sensing in cell populations. Physical review letters. 2017; 118(7):078101.

Fanelli D, McKane AJ. Diffusion in a crowded environment. Physical Review E. 2010; 82(2):021113.

572 **Gardiner CW**. Handbook of stochastic methods for physics, chemistry, and the natural sciences. 3rd ed.. ed.
573 Springer series in synergetics (Unnumbered), Berlin ; New York: Springer; 2004.

574 **Gierer A**, Meinhardt H. A theory of biological pattern formation. Kybernetik. 1972; 12(1):30–39.

575 **Gillespie DT**. The chemical Langevin equation. The Journal of Chemical Physics. 2000; 113(1):297–306.

576 **Gregor T**, Tank DW, Wieschaus EF, Bialek W. Probing the limits to positional information. Cell. 2007; 130(1):153–
577 164.

578 **Gregor T**, Wieschaus EF, McGregor AP, Bialek W, Tank DW. Stability and nuclear dynamics of the bicoid mor-
579 phogen gradient. Cell. 2007; 130(1):141–152.

580 **Grimm O**, Coppey M, Wieschaus E. Modelling the Bicoid gradient. Development. 2010; 137(14):2253–2264.

581 **Houchmandzadeh B**, Wieschaus E, Leibler S. Establishment of developmental precision and proportions in the
582 early Drosophila embryo. Nature. 2002; 415(6873):798.

583 **Huang H**, Kornberg TB. Myoblast cytonemes mediate Wg signaling from the wing imaginal disc and Delta-Notch
584 signaling to the air sac primordium. Elife. 2015; 4:e06114.

585 **Kanodia JS**, Rikhy R, Kim Y, Lund VK, DeLotto R, Lippincott-Schwartz J, Shvartsman SY. Dynamics of the Dorsal
586 morphogen gradient. Proceedings of the National Academy of Sciences. 2009; 106(51):21707–21712.

587 **Kicheva A**, Bollenbach T, Wartlick O, Jülicher F, Gonzalez-Gaitan M. Investigating the principles of morphogen
588 gradient formation: from tissues to cells. Current opinion in genetics & development. 2012; 22(6):527–532.

589 **Kicheva A**, Pantazis P, Bollenbach T, Kalaidzidis Y, Bittig T, Jülicher F, Gonzalez-Gaitan M. Kinetics of morphogen
590 gradient formation. Science. 2007; 315(5811):521–525.

591 **Kimmel CB**, Ballard WW, Kimmel SR, Ullmann B, Schilling TF. Stages of embryonic development of the zebrafish.
592 Developmental dynamics. 1995; 203(3):253–310.

593 **Kornberg TB**. Cytonemes and the dispersion of morphogens. Wiley Interdisciplinary Reviews: Developmental
594 Biology. 2014; 3(6):445–463.

595 **Kornberg TB**, Roy S. Cytonemes as specialized signaling filopodia. Development. 2014; 141(4):729–736.

596 **Lander AD**, Nie Q, Wan FY. Do morphogen gradients arise by diffusion? Developmental cell. 2002; 2(6):785–796.

597 **Liberman LM**, Reeves GT, Stathopoulos A. Quantitative imaging of the Dorsal nuclear gradient reveals limitations
598 to threshold-dependent patterning in Drosophila. Proceedings of the National Academy of Sciences. 2009;
599 106(52):22317–22322.

600 **Müller P**, Rogers KW, Jordan BM, Lee JS, Robson D, Ramanathan S, Schier AF. Differential diffusivity of Nodal
601 and Lefty underlies a reaction-diffusion patterning system. Science. 2012; 336(6082):721–724.

602 **Müller P**, Rogers KW, Shuizi RY, Brand M, Schier AF. Morphogen transport. Development. 2013; 140(8):1621–
603 1638.

604 **Rogers KW**, Müller P. Nodal and BMP dispersal during early zebrafish development. Developmental biology.
605 2018; .

606 **Rogers KW**, Schier AF. Morphogen gradients: from generation to interpretation. Annual review of cell and
607 developmental biology. 2011; 27:377–407.

608 **Sanders TA**, Llagostera E, Barna M. Specialized filopodia direct long-range transport of SHH during vertebrate
609 tissue patterning. Nature. 2013; 497(7451):628.

610 **Shvartsman SY**, Baker RE. Mathematical models of morphogen gradients and their effects on gene expression.
611 Wiley Interdisciplinary Reviews: Developmental Biology. 2012; 1(5):715–730.

612 **Stanganello E**, Scholpp S. Role of cytonemes in Wnt transport. J Cell Sci. 2016; 129(4):665–672.

613 **Teimouri H**, Kolomeisky AB. New model for understanding mechanisms of biological signaling: Direct transport
614 via cytonemes. The journal of physical chemistry letters. 2015; 7(1):180–185.

615 **Teimouri H**, Kolomeisky AB. Mechanisms of the formation of biological signaling profiles. Journal of Physics A:
616 Mathematical and Theoretical. 2016; 49(48):483001.

Tostevin F, Ten Wolde PR, Howard M. Fundamental limits to position determination by concentration gradients. PLoS computational biology. 2007; 3(4):e78.

Varennes J, Fancher S, Han B, Mugler A. Emergent versus individual-based multicellular chemotaxis. Physical review letters. 2017; 119(18):188101.

Wartlick O, Mumcu P, Kicheva A, Bittig T, Seum C, Jülicher F, Gonzalez-Gaitan M. Dynamics of Dpp signaling and proliferation control. Science. 2011; 331(6021):1154–1159.

Wilcockson SG, Sutcliffe C, Ashe HL. Control of signaling molecule range during developmental patterning. Cellular and Molecular Life Sciences. 2017; 74(11):1937–1956.

Yu SR, Burkhardt M, Nowak M, Ries J, Petrášek Z, Scholpp S, Schwille P, Brand M. Fgf8 morphogen gradient forms by a source-sink mechanism with freely diffusing molecules. Nature. 2009; 461(7263):533.

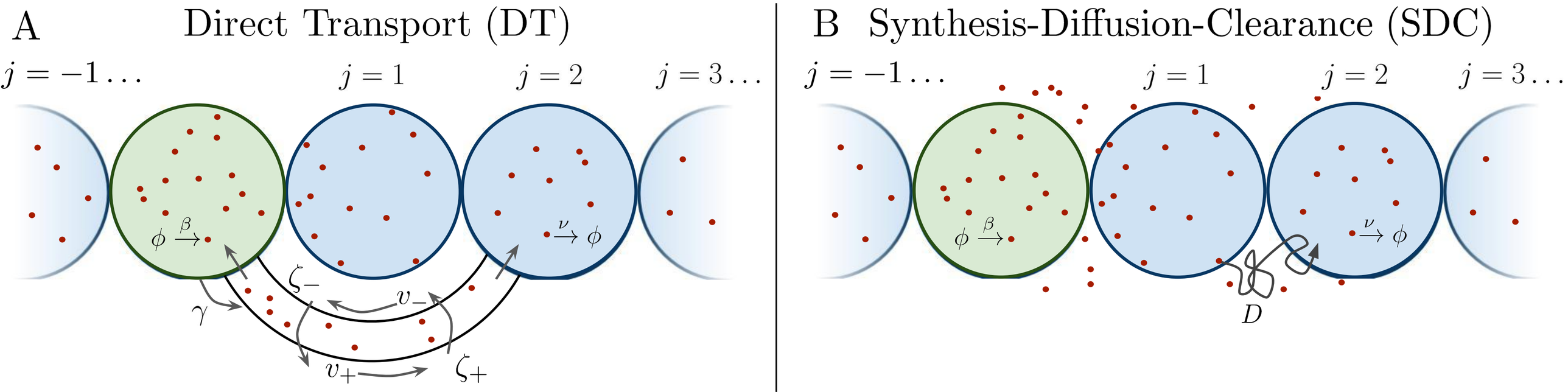
A
Direct Transport (DT)
$j=-1\ldots$
$j=1$
$j=2$
$j=3\ldots$
$\phi \xrightarrow{\beta}$
$\xrightarrow{\nu} \phi$
γ
ζ_-
v_-
v_+
ζ_+
B
Synthesis-Diffusion-Clearance (SDC)
$j=-1\ldots$
$j=1$
$j=2$
$j=3\ldots$
$\phi \xrightarrow{\beta}$
$\xrightarrow{\nu} \phi$
D

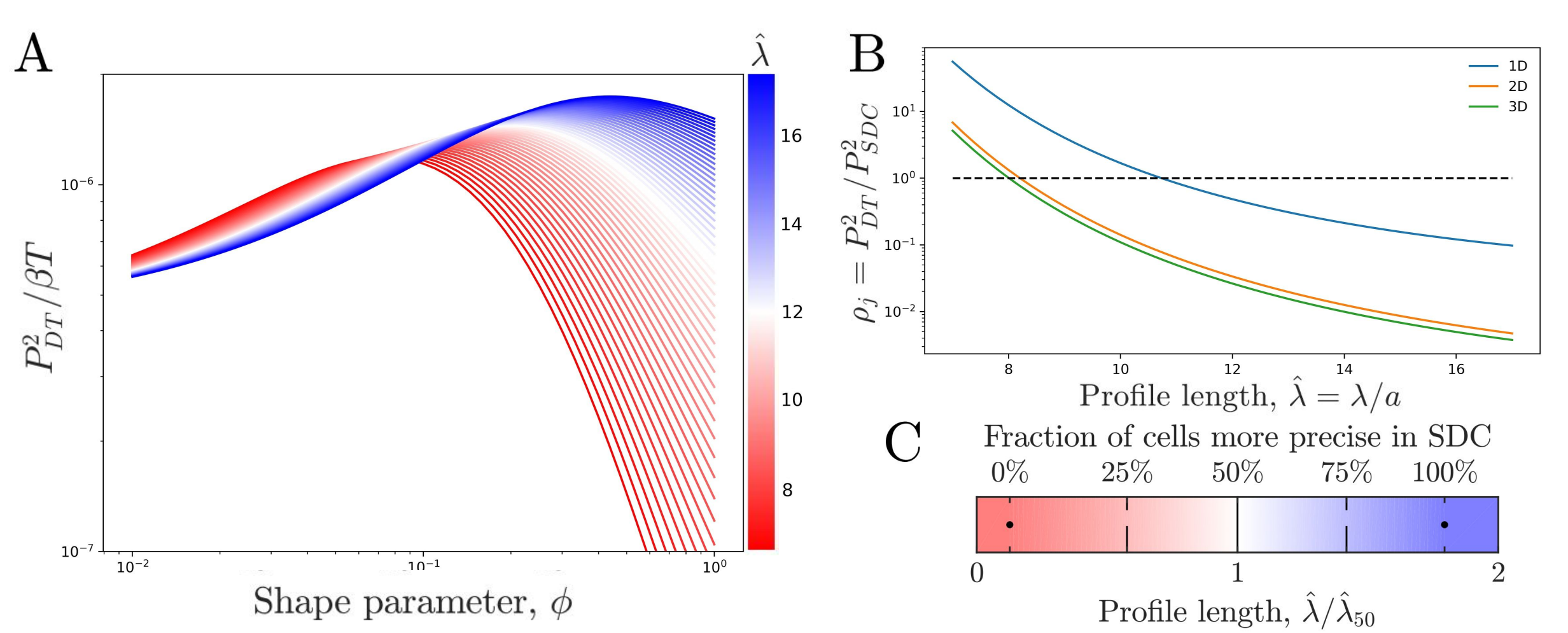
A
$\hat{\lambda}$
16
14
12
10
8
$P^2_{DT}/\beta T$
10^{-6}
10^{-7}
10^{-2}
10^{-1}
10^{0}
Shape parameter, ϕ
B
1D
2D
3D
$\rho_j = P^2_{DT}/P^2_{SDC}$
10^{1}
10^{0}
10^{-1}
10^{-2}
8
10
12
14
16
Profile length, $\hat{\lambda} = \lambda/a$
C
Fraction of cells more precise in SDC
0%
25%
50%
75%
100%
0
1
2
Profile length, $\hat{\lambda}/\hat{\lambda}_{50}$

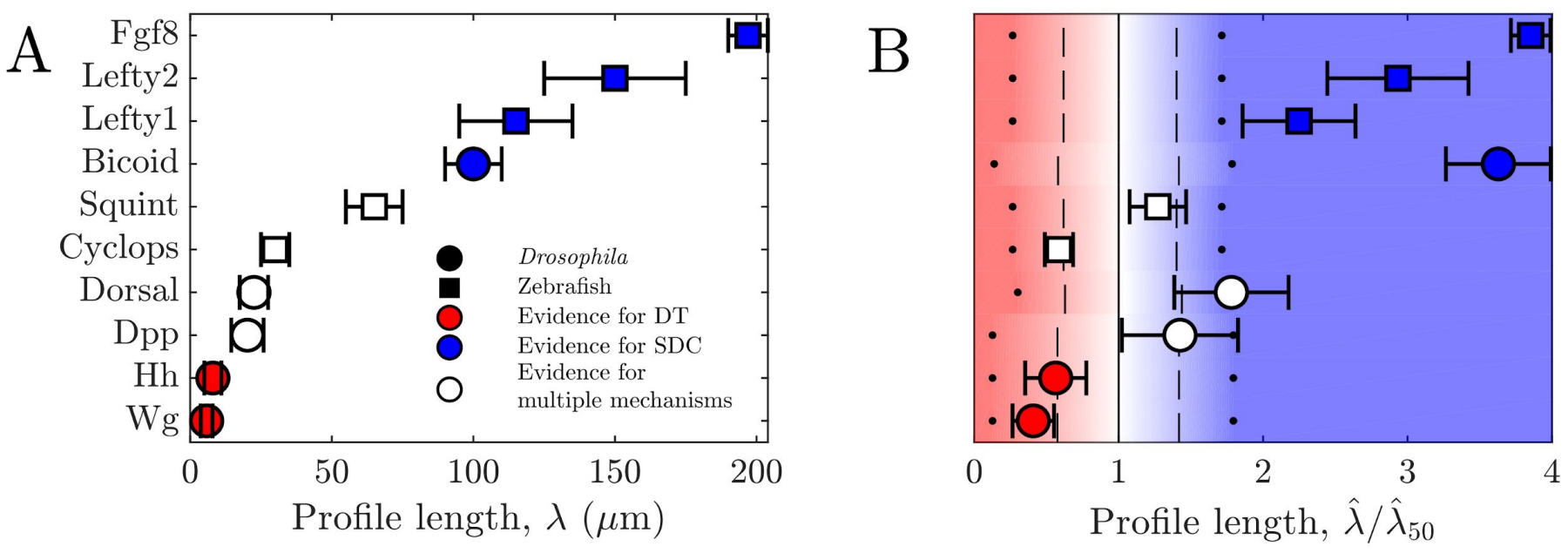
A
Fgf8
Lefty2
Lefty1
Bicoid
Squint
Cyclops
Dorsal
Dpp
Hh
Wg
Drosophila
Zebrafish
Evidence for DT
Evidence for SDC
Evidence for
multiple mechanisms
0
50
100
150
200
Profile length, λ (μm)
B
0
1
2
3
4
Profile length, λ̂/λ̂50